

# Effects of Elevated Pax6 Expression and Genetic Background on Mouse Eye Development



*Invest Ophthalmol Vis Sci*. Author manuscript; available in PMC 2010 March 01.

Published in final edited form as:
*Invest Ophthalmol Vis Sci*. 2009 September ; 50(9): 4045–4059. doi:10.1167/iovs.07-1630.

# Effects of Elevated Pax6 Expression and Genetic Background on Mouse Eye Development

**Simon A. Chanas**[1,2], **J. Martin Collinson**[3], **Thaya Ramaesh**[1,4,5], **Natalie Dorà**[3], **Dirk A. Kleinjan**[6], **Robert E. Hill**[6], and **John D. West**[1]

[1]Division of Reproductive and Developmental Sciences, Genes and Development Group, University of Edinburgh, Edinburgh, Scotland, United Kingdom

[3]School of Medical Sciences, College of Life Sciences and Medicine, University of Aberdeen, Institute of Medical Sciences, Aberdeen, Scotland, United Kingdom

[4]Department of Clinical and Surgical Sciences, Ophthalmology Section, University of Edinburgh, Princess Alexandra Eye Pavilion, Royal Infirmary of Edinburgh, Edinburgh, Scotland, United Kingdom

[6]Medical and Developmental Genetics Section, MRC Human Genetics Unit, Edinburgh, Scotland, United Kingdom.

## Abstract

**Purpose—**To analyze the effects of Pax6 overexpression and its interaction with genetic background on eye development.

**Methods—**Histologic features of eyes from hemizygous *PAX77*$^{+/-}$ transgenic (high *Pax6* gene dose) and wild-type mice were compared on different genetic backgrounds. Experimental *PAX77*$^{+/-}$↔wild-type and control wild-type↔wild-type chimeras were analyzed to investigate the causes of abnormal eye development in *PAX77*$^{+/-}$ mice.

**Results—***PAX77*$^{+/-}$ mice showed an overlapping but distinct spectrum of eye abnormalities to *Pax6*$^{+/-}$ heterozygotes (low *Pax6* dose). Some previously reported *PAX77*$^{+/-}$ eye abnormalities did not occur on all three genetic backgrounds examined. Several types of eye abnormalities occurred in the experimental *PAX77*$^{+/-}$↔wild-type chimeras, and they occurred more frequently in chimeras with higher contributions of *PAX77*$^{+/-}$ cells. Groups of RPE cells intruded into the optic nerve sheath, indicating that the boundary between the retina and optic nerve may be displaced. Both *PAX77*$^{+/-}$ and wild-type cells were involved in this ingression and in retinal folds, suggesting that neither effect was cell-autonomous. Cell-autonomous effects included failure of *PAX77*$^{+/-}$ and wild-type cells to mix normally and overrepresentation of *PAX77*$^{+/-}$ in the lens epithelium and RPE.

**Conclusions—**The extent of *PAX77*$^{+/-}$ eye abnormalities depended on *PAX77*$^{+/-}$ genotype, genetic background, and stochastic variation. Chimera analysis identified two types of cell-autonomous effects of the *PAX77*$^{+/-}$ genotype. Abnormal cell mixing between *PAX77*$^{+/-}$ and



Corresponding author: John D. West, Division of Reproductive and Developmental Sciences, Genes and Development Group, University of Edinburgh, Hugh Robson Building, George Square, Edinburgh EH8 9XD, Scotland, UK; john.west@ed.ac.uk..
[2]Present affiliation: Division of Cancer Studies, University of Birmingham, Cancer Research UK Institute for Cancer Studies, Birmingham, United Kingdom
[5]Present affiliation: Division of Reproductive and Developmental Sciences, Centre for Reproductive Biology, University of Edinburgh, Queen's Medical Research Institute, Edinburgh Scotland, United Kingdom.

Disclosure: **S.A. Chanas**, None; **J.M. Collinson**, None; **T. Ramaesh**, None; **N. Dorà**, None; **D.A. Kleinjan**, None; **R.E. Hill**, None; **J.D. West**, None

wild-type cells suggests altered expression of cell surface adhesion molecules. Some phenotypic differences between *PAX77*$^{+/-}$↔wild-type and *Pax6*$^{+/-}$↔wild-type chimeras may reflect differences in the levels of *PAX77*$^{+/-}$ and *Pax6*$^{+/-}$ contributions to chimeric lenses.

The eye develops from three major sources of cells. The surface ectoderm of the head produces the lens and the corneal, limbal, and conjunctival epithelia. The neuroectoderm produces the neural retina and retinal pigment epithelium (RPE), and extensions of both these tissues cover the ciliary body, ciliary process, and iris. The periocular mesenchyme, comprising mesoderm and neural crest–derived mesectoderm cells, produces the choroid, sclera, corneal stroma, corneal endoderm, and stroma of the ciliary body, ciliary process, and iris.1

The transcription factor Pax6 is essential for normal eye development in vertebrates.2-6 During development *Pax6* is expressed in the developing lens; conjunctival, limbal and corneal epithelia; neural retina; RPE; ciliary body; and iris.4,5 After birth, *Pax6* is downregulated in many eye tissues, but expression continues in the amacrine cells of the retina and the lens and in the conjunctival, limbal, and corneal epithelia.5,7,8

Homozygous *Pax6*$^{-/-}$ mice, with two nonfunctional alleles, die at birth with no eyes or nose and with brain abnormalities.5,9-11 In some cases they have abnormal dentition but the penetrance of this effect is highly dependent on the genetic background.12 Human *PAX6*$^{-/-}$ homozygotes or compound heterozygotes are rare and the condition is lethal, causing anophthalmia with severe craniofacial and central nervous system defects.13

Heterozygous *Pax6*$^{+/-}$ mice and *PAX6*$^{+/-}$ humans produce low levels of Pax6 and are viable and fertile but have a range of eye abnormalities.2 In *Pax6*$^{+/-}$ mice, abnormal eye development commonly results in small eyes, iris hypoplasia, cataracts, a thin corneal epithelium with fewer cell layers, corneal opacity, failure of the lens to separate completely from the corneal epithelium, and glaucoma. Other developmental abnormalities, including retinal dysplasia, coloboma, abnormal cell accumulation in the vitreous, and adhesions between the lens and cornea (keratolenticular strands) or between the iris and cornea (iridocorneal synechia), may also occur.10,14-18 Adult *Pax6*$^{+/-}$ mice also show progressive corneal deterioration. The corneal epithelium is thin and fragile and goblet cells accumulate; the stroma becomes vascularized from the periphery and infiltrated with inflammatory cells.16,19

Human *PAX6*$^{+/-}$ heterozygotes usually have normal-sized eyes but otherwise show a range of abnormalities similar to those in *Pax6*$^{+/-}$ mice. Clinical conditions associated with *PAX6*$^{+/-}$ heterozygosity include aniridia (absent or hypoplastic iris), Peters' anomaly (keratolenticular adhesions with loss of posterior cornea), iridolenticular adhesions, iridocorneal adhesions, cataract, corneal opacity, congenital nystagmus, and foveal hypoplasia.2,3,13,20,21 Postnatal changes include early-onset glaucoma, corneal vascularization, corneal infiltration by inflammatory cells (autosomal dominant keratitis), and accumulation of goblet cells in the corneal epithelium. The corneal epithelium is not maintained adequately, and this is thought to involve a deficiency of limbal stem cells.22

Eye development seems to be unusually sensitive to Pax6 dosage and both *PAX6* gene duplication in humans23 and experimentally induced high expression levels in the mouse24 can also cause eye abnormalities. *PAX77*$^{+/-}$ transgenic mice are hemizygous for five to six copies of a human *PAX6* yeast artificial chromosome (YAC) inserted at a single locus.24 The YAC contains the human *PAX6* gene with all the enhancer and promoter elements. The amino acid sequence of human PAX6 is identical with mouse Pax6 and the human *PAX6* regulatory elements are fully functional in mouse, so that the transgene is expressed in an appropriate tissue-specific manner and fully functional.24




Europe PMC Funders Author Manuscripts

The extra copies of *PAX6* can compensate for the Pax6 deficiencies in both $Pax6^{-/-}$ and $Pax6^{+/-}$ mice. On a wild-type $Pax6^{+/+}$ genetic background, however, this overexpression of Pax6 in $PAX77^{+/-}$ mice results in eye abnormalities, which overlap with those seen in $Pax6^{+/-}$ mice. These hemizygous $PAX77^{+/-}$ $Pax6^{+/+}$ mice often had microphthalmia, small corneas; flat irides; abnormal, small or absent ciliary bodies; small abnormal lenses; and abnormal photoreceptors, but the phenotype was variable.

Pax6 has multiple pleiotropic roles in cell proliferation, migration, adhesion, and signaling25 and may act cell-autonomously or nonautonomously. Experimental studies have identified several primary cell-autonomous roles for Pax6 that underlie the eye abnormalities in homozygous $Pax6^{-/-}$ mice.6,26-30 Some of the eye abnormalities in heterozygous $Pax6^{+/-}$ mice are caused by nonautonomous effects and may be secondary to primary affects of low Pax6 in the surface ectoderm and lens.14,15 Nonautonomous effects probably also underlie some of the defects caused by abnormal migration of neural crest cells18 but cell-autonomous effects may also be involved because Pax6 appears to be expressed transiently in the corneal stroma,17 and chimera experiments indicate that Pax6 acts cell-autonomously in this tissue.28

Analysis of mouse chimeras has been used successfully to distinguish between the cell-autonomous and nonautonomous effects of $Pax6^{-/-}$ and $Pax6^{+/-}$ genotypes on eye development.14,26-28 One important observation to emerge from studies of $Pax6^{+/-}$↔wild-type chimeras was that $Pax6^{+/-}$ cells were excluded from the lens epithelium of $Pax6^{+/-}$↔wild-type chimeras by embryonic day (E)16.5. Although $Pax6^{+/-}$ cells contributed to tissues of the anterior segment, the chimeras did not show iris hypoplasia or other anterior segment abnormalities that occur in nonchimeric $Pax6^{+/-}$ mice. This exclusion of $Pax6^{+/-}$ cells from the lens epithelium is interpreted as a cell-autonomous effect, and it produces an almost entirely wild-type lens. It was further proposed that the largely wild-type lens cells exerted a nonautonomous effect on the anterior segment and prevented the formation of anterior segment abnormalities.14 One of the purposes of this study was to determine whether $PAX77^{+/-}$ cells are similarly excluded from the lens.

In the present study, we first examined the range of eye abnormalities caused by the $PAX77^{+/-}$ genotype on different genetic backgrounds. We then analyzed fetal $PAX77^{+/-}$↔wild-type chimeras to investigate the underlying developmental causes of these eye abnormalities and distinguish between cell-autonomous and nonautonomous effects of elevated Pax6 expression in the eye. The use of these chimeras to demonstrate a cell-autonomous effect of increased Pax6 expression in the neurocortex has been reported elsewhere.31 Both low levels of Pax6 in $Pax6^{+/-}$ heterozygotes and high levels in $PAX77^{+/-}$ transgenics cause lens abnormalities, and so we specifically wanted to use chimeras to test the hypothesis that $PAX77^{+/-}$ cells would be depleted or excluded from the lens epithelium, like $Pax6^{+/-}$ cells in our $Pax6^{+/-}$↔wild-type chimeras.

## Materials and Methods

### Mice

Transgenic *PAX77* mice on an outbred CD1 background were a kind gift from Veronica van Heyningen (MRC Human Genetics Unit, Edinburgh) and were produced in her laboratory.24 The *PAX77* transgene was maintained on an outbred albino CD1A background (homozygous $Gpi1^{a/a}$, CD1 strain) and also crossed to inbred CBA/Ca mice. Outbred CD1 and inbred CBA/Ca, BALB/c, and A/J strain mice were obtained from Bantin & Kingman (Aldbrough, UK) and Harlan Olac (Bicester, UK). The mice were bred and maintained in the Medical Faculty Animal Area at the University of Edinburgh. Animal work was

performed in accordance with U.K. institutional guidelines, Home Office regulations, and the ARVO Statement for the Use of Animals in Ophthalmic and Vision Research.

## Chimera Production

Two series of E16.5 chimeric fetuses (series SCA and SCB) were generated by aggregation of eight-cell-stage embryos, as described previously,32 based on the original method of Tarkowski.33 One of each pair of aggregated embryos was hemizygous ($Tg^{+/-}$) for the *TgN(Hbb-b1)* reiterated $\beta$-globin transgenic sequence that can be identified by DNA in situ hybridization on histologic sections and acts as a lineage marker.34,35 The aggregated embryos also differed at the albino locus (*Tyr*) and for *Gpi1*, encoding glucose phosphate isomerase. Each series produced $PAX77^{+/-}$↔wild-type ($PAX77^{-/-}$) experimental chimeras and wild-type ($PAX77^{-/-}$)↔wild-type ($PAX77^{-/-}$) control chimeras. The genotype combinations for the experimental chimeras were $PAX77^{+/-}$, $Gpi1^{a/a}$, $Tyr^{c/c}$, $Tg^{-/-}$↔$PAX77^{-/-}$, $Gpi1^{b/b}$, $Tyr^{+/+}$, and $Tg^{+/-}$ in series SCA and $PAX77^{+/-}$, $Gpi1^{b/b}$, $Tyr^{+/+}$, $Tg^{+/-}$↔$PAX77^{-/-}$, $Gpi1^{a/a}$, $Tyr^{c/c}$, and $Tg^{-/-}$ in series SCB.

For series SCA, crosses between CD1A females and CD1A-$PAX77^{+/-}$ males produced $PAX77^{+/-}$ and $PAX77^{-/-}$ eight-cell stage embryos, all of which were $Gpi1^{a/a}$, $Tyr^{c/c}$, and $Tg^{-/-}$. These embryos were aggregated to $PAX77^{-/-}$, $Gpi1^{b/b}$, $Tyr^{+/+}$, and $Tg^{+/-}$ eight-cell embryos produced from crosses between (C57BL/6 × CBA/Ca)F1 females ($Gpi1^{b/b}$, $Tyr^{+/+}$, and $Tg^{+/+}$) and males from stock BTC that were $Gpi1^{b/b}$, pigmented ($Tyr^{+/+}$), and homozygous for the transgenic lineage marker ($Tg^{+/+}$) on a largely (C57BL/6 × CBA/Ca)F1 genetic background. In $PAX77^{+/-}$↔wild-type experimental chimeras from series SCA, the transgenic lineage marker was carried by the wild-type embryo.

The $PAX77^{+/-}$ transgene was backcrossed for five generations onto the CBA/Ca inbred strain to produce series SCB chimeras. In this series, the embryos from the $PAX77^{+/-}$ × $PAX77^{-/-}$ cross were positively labeled with the $\beta$-globin marker transgene. For series SCB, eight-cell embryos were obtained from crosses between CBA-$PAX77^{+/-}$ females and BTC males to produce $PAX77^{+/-}$ and $PAX77^{-/-}$ embryos, all of which were $Gpi1^{b/b}$, $Tyr^{+/+}$, and $Tg^{+/-}$. These embryos were aggregated to $PAX77^{-/-}$, $Gpi1^{+/+}$, $Tyr^{c/c}$, and $Tg^{-/-}$ embryos produced from intercrosses between (BALB/c × A/J)F1 females and (BALB/c × A/J)F1 males.

For each series, chimeras were produced as described previously,32 except that embryos were cultured in either M1636 or KSOM37,38 culture medium and handled in either M239 or KSOM-H40 handling medium. Females were superovulated and mated to appropriate males. Eight-cell stage embryos were collected, denuded of their zonae pellucidae, and aggregated in the combinations described herein. After overnight culture, the E3.5 aggregated embryos were surgically transferred to the uteri of E2.5 pseudopregnant $Gpi1^{c/c}$ females (hybrid stock CF132) and recovered at E16.5 (which was timed with respect to the recipient female).

## Analysis of Chimeras

The recipient females were killed at E16.5, and the fetuses were dissected into cold PBS. GPI1 electrophoresis was performed on limb and tail tissue, and scanning densitometry was used to estimate the global chimeric composition as percentage of GPI1-A and percentage of GPI1-B, as described previously.32 Any maternal contamination would have been represented as a GPI1-C band, which was excluded from the analysis. Heads were fixed and embedded in paraffin wax for analysis of the compositions of specific eye tissues by DNA-DNA in situ hybridization to detect the $\beta$-globin transgenic lineage marker.35 The fetal torsos were digested to obtain DNA for PCR genotyping to distinguish between control

wild-type (*PAX77*$^{-/-}$)↔wild-type (*PAX77*$^{-/-}$) and experimental *PAX77*$^{+/-}$↔wild-type (*PAX77*$^{-/-}$) chimeras.

For DNA-DNA in situ hybridization, fetal heads were sectioned coronally at 7 $\mu$m and mounted on slides coated with 3-aminopropyltriethoxysilane (Sigma-Aldrich, Poole, UK) and subjected to in situ hybridization with a digoxigenin labeled probe for the $\beta$-globin transgene, as described previously35 with the amendment that, after dewaxing, the slides were placed in 10 mM sodium citrate and microwaved at full power four times for 5 minutes each before being allowed to cool for 30 minutes. Hybridized probe was detected by diaminobenzidine (DAB) staining for peroxidase labeled antibody (polyclonal sheep anti-digoxigenin Fab fragments conjugated to horseradish peroxidase; Roche, Welwyn Garden City, UK). The slides were counterstained with hematoxylin, and the percentage of transgene-positive cells in each of the selected tissues was estimated in the chimeric embryo heads by counting nuclei with and without a hybridization signal under phase contrast light microscopy. Typically between 200 and 500 nuclei were scored as *Tg*-positive or -negative. Not all *Tg*$^{+/-}$ nuclei produce the expected hybridization signal, because only part of the nucleus may be included in the section.35 Consequently, the percentage *Tg*-positive cells was corrected with a tissue-specific correction factor determined by the percentage of *Tg*-positive cells present in eye tissues of E16.5 *Tg*$^{+/-}$-positive control fetuses from (C57BL/6 × CBA/Ca) × BTC crosses.

For *PAX77*$^{+/-}$↔wild-type experimental chimeras in series SCA the global *PAX77*$^{+/-}$ contribution was estimated as the percentage GPI1-A, and the *PAX77*$^{+/-}$ contributions to specific eye tissues were estimated from the corrected percentage of *Tg*-negative cells (or uncorrected percentage of albino cells for the RPE). Contributions to specific tissues were evaluated by comparing the corrected percentage *Tg*-negative/GPI1-A ratios (observed/expected ratios) for experimental and control chimeras. Underrepresentation of *PAX77*$^{+/-}$ cells in specific tissue would produce a significantly lower observed/expected ratio in experimental chimeras than control chimeras. For *PAX77*$^{+/-}$↔wild-type experimental chimeras in series SCB the global *PAX77*$^{+/-}$ contribution was estimated as percentage of GPI1-B and the *PAX77*$^{+/-}$ contributions to specific eye tissues were estimated from the corrected percentage of *Tg*-positive cells (or uncorrected percentage of pigmented cells in the RPE). For this series of chimeras, underrepresentation of *PAX77*$^{+/-}$ cells in a specific tissue would produce a significantly lower corrected percentage *Tg*-positive/GPI1-B ratio (observed/expected ratio) in experimental chimeras than control chimeras.

## Histology

Twelve-week-old mice were killed by cervical dislocation and the eyes were removed, weighed, and fixed in Bouin's solution overnight at 4°C. After fixation, the lens was removed from most eyes via a hole cut in the posterior to facilitate sectioning. (If left intact, the brittle lenses often shatter during sectioning, and fragments can obscure other tissues.) The eyes were dehydrated in alcohols and embedded in paraffin wax and 7-$\mu$m microtome sections were cut along the anterior-posterior axis. Fetuses were decapitated, and heads were fixed in 3:1 ethanol/acetic acid overnight at 4°C, dehydrated, and embedded in paraffin wax, and 7-$\mu$m coronal sections were cut. Sections were mounted onto slides and stained with hematoxylin and eosin according to standard histologic procedures. For PAS staining, the slides were treated with periodic acid and then stained with Schiff's reagent.

## Immunohistochemistry

Embryos were fixed in 4% wt/vol paraformaldehyde, dehydrated, and embedded in paraffin wax. The 7-$\mu$m sections were dewaxed and rehydrated. Antigen retrieval and immunohistochemistry was performed simultaneously on control and transgenic sections as

described in Collinson et al.28 Pax6/PAX6 staining levels in *PAX77*$^{+/-}$ and *PAX77*$^{-/-}$ (wild-type) eyes were quantified by a modification of the protocol described in Song et al.41 To control for variability of immunostaining efficiency between sections and samples, AP2$\alpha$ staining was used as an internal control, and Pax6 levels were expressed as a ratio relative to AP2$\alpha$ labeling intensity. Wax sections of E14.5 eyes were rehydrated, and antigen retrieval performed by boiling in 0.01 M citrate buffer (pH 6) 20 minutes. The sections were simultaneously double-labeled for Pax6 and AP2$\alpha$ with the PAX6 (1:40 dilution) and 3b5 (1:40 dilution) monoclonal antibodies, respectively, obtained from the Developmental Studies Hybridoma Bank (developed under the auspices of the National Institute of Child Health and Human Development, Bethesda, MD, and maintained by the University of Iowa, Iowa City). Secondary antibodies were Alexa Fluor-488 labeled goat anti-mouse IgG1 for Pax6 and Alexa Fluor-594 labeled goat anti-mouse IgG2b for AP2$\alpha$ (1:300 dilution for both; Invitrogen, Paisley, UK). *PAX77*$^{+/-}$ and wild-type samples were processed identically and immunostained side-by-side. After mounting, fluorescence photographs were taken in monochrome using a camera (QICAM Fast1394) with identical exposure settings within commercial software (Volocity 4; ImproVision, Coventry, UK). Both Pax6 and AP2$\alpha$ images were captured from each field, and underexposed to avoid burnout. Images were exported as unprocessed .tif files into image-analysis software (Photoshop 7; Adobe Systems, San Jose, CA) and the Pax6 and AP2$\alpha$ fluorescence intensity of sections of the lens epithelium was measured using the histogram tool (Luminosity; Adobe Systems). Pax6 and AP2$\alpha$ luminosities were measured at identical sites on each lens epithelium, and a mean Pax6/AP2$\alpha$ ratio determined for each lens. The increase in Pax6 protein levels in *PAX77*$^{+/-}$ lenses was then calculated by dividing the mean Pax6/AP2$\alpha$ value for *PAX77*$^{+/-}$ lenses by the mean Pax6/AP2$\alpha$ value for wild-type lenses, separately for each genetic background.

### *PAX77* Genotyping by PCR Analysis of Genomic DNA

PCR was performed on genomic DNA from digested mouse tail tips or fetal torsos. Tissues were digested overnight at 55°C in 1× digestion buffer (10 mM Tris [pH 7.8], 50 mM KCl, 5 mM $MgCl_2$, 0.45% Igepal, 0.45% Tween-20, and 0.1 mg/mL gelatin) with 0.6 mg/mL freshly prepared proteinase K added. The following day, the proteinase K was inactivated by heating the tubes at 100°C for 5 to 10 minutes. The tubes were then briefly centrifuged at 12,000*g* to pellet precipitates, and the solution was removed to a fresh tube. Genomic DNA was stored at −20°C until required.

Two separate pairs of primers were used to amplify a 282-bp region of transgenic human *PAX6* and a 398-bp region of mouse *Pax6* which can be resolved using agarose gel electrophoresis. The sequences of the primers used to amplify the mouse *PAX6* region were 5′-GAGGGTTTCCTGGATCTGG-3′ and 5′-CGCAAATACACCTTTGCTCA-3′ for the forward and reverse primers, respectively. The sequences of the primers used to amplify the human *PAX6* transgene were 5′-CACGGTTTACTGGGTCTGG-3′ and 5′-CCGTGTGCCTCAACCGTA-3′ for the forward and reverse primers, respectively. A volume of 1 $\mu$L of genomic DNA was added to a PCR reaction of 50-$\mu$L total volume containing 1× *Taq* buffer, 1.5 mM $MgCl_2$, 200 ng of each primer, 10 nM of each dNTP, and 2.5 units of *Taq* DNA polymerase (Roche). The reactions were subjected to 30 cycles of 95°C for 1 minute, 57.5°C for 45 seconds, and 72°C for 45 seconds. A volume of 2 $\mu$L 6× DNA loading buffer (0.25% bromophenol blue, 15% Ficoll 400; Roche) was added to 12 $\mu$L of each PCR reaction, and the DNA was subjected to gel electrophoresis in a 2% agarose gel containing 1× TAE (40 mM Tris [unbuffered], 0.2 mM EDTA, and 0.1% acetic acid) and 0.6 $\mu$g/mL ethidium bromide. Electrophoresis proceeded at 100 V for between 1 and 2 hours. The DNA was then viewed by placing the gel under UV light with a wavelength of 320 nm. Both human *PAX6* and mouse *Pax6* DNA fragments were amplified from the DNA

of mice carrying the *PAX77* transgene, whereas only the mouse *Pax6* fragment was amplified from wild-type mice and control chimeras.

## Results

### Reduced Eye Size Caused by Interactions between Genetic Background and *PAX77* Genotype

Microphthalmia was the most noticeable external phenotype in our founder $PAX77^{+/-}$ transgenic mice, and this characteristic was retained when $PAX77^{+/-}$ was maintained on a similar outbred CD1 genetic background. Overall, 4/29 (14%) of these CD1-$PAX77^{+/-}$ mice, whose genotype was confirmed by PCR, were anophthalmic and the others were all severely microphthalmic. On this genetic background, the wet mass of $PAX77^{+/-}$ eyes ranged from 1.2 to 11.3 mg. Figure 1A shows that the mean mass was reduced to only 22% of the wild-type mean at 12 weeks—a highly significant difference.

CD1-$PAX77^{+/-}$ males were crossed to inbred CBA/Ca females to produce (CBA/Ca × CD1)F1-$PAX77^{+/-}$ (hereafter abbreviated to F1-$PAX77^{+/-}$) mice. On this F1 hybrid genetic background, there was no significant difference in eye size and the mean mass of $PAX77^{+/-}$ eyes was 95% of the wild-type mean. The eye size was reduced after further backcrosses to inbred CBA/Ca mice to produce partially congenic CBA-$PAX77^{+/-}$ mice, and by the fifth-generation (N5) the mean mass of $PAX77^{+/-}$ eyes was significantly reduced to 60% of the wild-type mean (Fig. 1A). Thus, both the penetrance and expressivity of the $PAX77^{+/-}$ microphthalmia phenotype was dependent on genetic background; the expressivity differed on CBA and CD1 genetic backgrounds and on an F1 genetic background the phenotype was rarely penetrant. (The overlap between F1 and F1-$PAX77^{+/-}$ eye sizes was demonstrated by the observation that at 12 weeks, 38 of 43 F1-$PAX77^{+/-}$ eyes were heavier than the lightest wild-type F1 eye, and 19 of 43 F1-$PAX77^{+/-}$ eyes exceeded the wild-type F1 median eye mass.) Analysis of variance showed a highly significant interaction between genotype and genetic background for the mean eye mass of each mouse ($P < 0.001$), confirming that the effect of the $PAX77^{+/-}$ genotype depends on the genetic background.

The wet mass of the CBA-$PAX77^{+/-}$ eyes ranged from 5.0 to 31.4 mg and varied not only among mice, but also between eyes in individual mice (Fig. 1B). The percentage coefficient of variation of eye mass was below 20% for all three groups of wild-type mice (7.2%, 10.5%, and 4.4% for CD1, F1, and CBA genetic backgrounds, respectively) but was higher in CBA-$PAX77^{+/-}$ (48.2%) and CD1-$PAX77^{+/-}$ (39.6%) than in F1-$PAX77^{+/-}$ (18.28%) mice. The within-mouse differences in wet mass between left and right eyes (Fig. 1B) were consistently low in wild-type mice on all three genetic backgrounds and F1-$PAX77^{+/-}$ mice but statistically significant for CD1- and CBA-$PAX77^{+/-}$ mice. Neither the left nor the right eyes were consistently heavier. The differences between eyes were greater for CBA-$PAX77^{+/-}$ than CD1-$PAX77^{+/-}$, but this is partly because CD1-$PAX77^{+/-}$ eyes were much smaller and partly because mice with no eyes or eyes that were too small to weigh were excluded so the CD1-$PAX77^{+/-}$ variation is underestimated. The percentage difference provides a relative measure of variation that is less affected by differences in overall mean eyemass (Fig. 1C) and this shows larger percentage differences between left and right eyes in CBA-$PAX77^{+/-}$ and CD1-$PAX77^{+/-}$ than in F1-$PAX77^{+/-}$ mice.

### Histologic Evaluation of Genetic Background Effects on Adult $PAX77^{+/-}$ Eye Abnormalities

Figures 2A–D show representative normal histologic features in adult wild-type CBA mouse eyes. Histologic examination of the lens and the vitreous was not performed because the lenses were removed from all the wild-type eyes (see the Materials and Methods section). Histologic features were entirely normal in wild-type eyes on all three genetic backgrounds

except that outbred CD1 mice are albino (*Tyr*$^{c/c}$) and some CD1 eyes had no outer nuclear layer in the neural retina. The latter abnormality is characteristic of mice homozygous for the common *Pde6b*$^{rd1}$ allele, which causes retinal degeneration. This allele is absent from the inbred CBA/Ca strain that we used and the histology of the outer nuclear layer was entirely normal. The major effects of the genetic background on the range of *PAX77*$^{+/-}$ morphologic abnormalities are summarized in Table 1 and are described in the following sections.

F1-*PAX77*$^{+/-}$ mice, whose genotype was verified by PCR, displayed a less severe eye phenotype than CD1-*PAX77*$^{+/-}$ or CBA-*PAX77*$^{+/-}$ mice. Histologic analysis of 14 F1-*PAX77*$^{+/-}$ eyes, mostly with lenses removed, revealed several consistent abnormalities that were absent from wild-type F1 littermates. F1-*PAX77*$^{+/-}$ eyes had smaller corneas than normal (Figs. 2A, 2E) but there were no other obvious corneal abnormalities (Fig. 2G). The iris contained cystlike structures (11/14 cases), and the ciliary body was disorganized and small compared with that in their wild-type littermates (Fig. 2F). The retinal pigmented epithelium (RPE) appeared normal, but the neural retina was sometimes disorganized, particularly in the outer nuclear layer (ONL); Figure 2H shows a minor abnormality.

Histologic analysis of eight CBA-*PAX77*$^{+/-}$ eyes revealed a variable phenotype that was intermediate between that of CD1-*PAX77*$^{+/-}$ and F1-*PAX77*$^{+/-}$ mice (Table 1). The corneal diameter of the CBA-*PAX77*$^{+/-}$ eyes was usually disproportionately reduced, relative to the eye diameter, compared with that of wild-type CBA eyes (Figs. 2I–2E), but the corneal epithelium thickness was not significantly affected (Figs. 2C, 2K). In contrast to *Pax6*$^{+/-}$ heterozygotes,16 no goblet cells were identified in *PAX77*$^{+/-}$ corneal epithelia stained with hematoxylin and eosin (Figs. 2G, 2K, 2N) or PAS (Fig. 2R and data not shown). The iris was thickened and cystic (Fig. 2J) and the ciliary bodies were either absent or disorganized and small (Fig. 2J). The retina appeared thinner (6/8 eyes) and the inner and outer nuclear layers were disorganized (4/8 eyes) and often contained rosettes (Fig. 2L). Lenses were left in situ in some (3/8 eyes) CBA-*PAX77*$^{+/-}$ eyes to allow histologic examination. Lenses were small relative to the size of the eyes, and all contained cataracts. The anterior chamber and the vitreous usually contained eosinophilic material (7/8 eyes; Fig. 2L).

Inspection of the intact CD1-*PAX77*$^{+/-}$ eyes with a dissecting microscope showed that they all had lens opacities (cataracts). Histologic analysis of 13 CD1-*PAX77*$^{+/-}$ eyes revealed a more severe phenotype than either CBA-*PAX77*$^{+/-}$ or F1-*PAX77*$^{+/-}$ eyes (Table 1), which included severe microphthalmia and significant morphologic abnormalities in several eye tissues (Figs. 2M–T). Corneal diameters were small but not disproportionately so in the smallest CD1-*PAX77*$^{+/-}$ eyes. In all CD1-*PAX77*$^{+/-}$ eyes, the iris was malformed, thicker than both wild-type and CBA-*PAX77*$^{+/-}$ irides, and displayed adhesions and sometimes cystlike cavities (7/13; Fig. 2N). The ciliary bodies were disorganized in all eyes, and some had a persistent pupillary membrane (Figs. 2O, 2Q, 2R). CD1-*PAX77*$^{+/-}$ lenses, left in situ for histology, were small and often vacuolated (Fig. 2S), and the lens capsule, demonstrated by PAS staining, was thickened, wrinkled (6/13), and adherent to the adjacent tissues (Fig. 2R). Densely packed cells with epithelial morphology formed multiple layers beneath the capsule in all CD1-*PAX77*$^{+/-}$ eyes examined (implying subcapsular epithelial cell proliferation; Fig. 2Q) and were also sometimes seen between differentiated lens fibers. Retinas showed several abnormalities (Figs. 2P, 2S, 2T); most were dysplastic (10/13) and contained rosettes (7/13), and some were folded (4/13) and/or adherent to the lens capsule (10/13), but they were still arranged in recognizable layers. Occasional absence of the outer nuclear layer was attributed to homozygosity for a retinal degeneration allele (e.g., *Pde6b*$^{rd1}$) rather the *PAX77* genotype, because it also occurred in some control, wild-type CD1 animals. Sometimes the vitreous cavity was not detectable (3/13), as the retina adhered to the entire posterior lens capsule (Fig. 2M). In one of these eyes, the anterior chamber was

also absent, because the iris was adherent to the cornea and anterior lens capsule. Less frequently, some CD1-*PAX77*$^{+/-}$ eyes contained an ectopic ball of retinal cells, possibly retinal ganglion cells, between the retina and lens (Fig. 2T). The anterior chamber and the vitreous often contained eosinophilic material (Figs. 2N, 2O) similar to that seen in CBA-*PAX77*$^{+/-}$ eyes.

## Genetic Background Effects on Fetal *PAX77*$^{+/-}$ Eye Abnormalities

Eye histology was examined in coronal sections of the heads of E16.5 fetuses on the two most extreme genetic backgrounds (CD1 and F1) to compare wild-type CD1 ($n = 6$; Figs. 3A, 3B), wild-type F1 ($n = 6$; Fig. 3C), CD1-*PAX77*$^{+/-}$ ($n = 8$; Figs. 3D–F), and F1-*PAX77*$^{+/-}$ ($n = 6$; Figs. 3G–I) eyes. Although the anterior segment appeared similar in wild-type embryos on both genetic backgrounds, the vitreous showed some differences. In the E16.5 wild-type F1 mice, most of the hyaloid system had disappeared from the vitreous, and the blood vessels were mainly located on the surface of the lens and on the inner surface of the retina, but persistent small clumps of cells were detected in some wild-type CD1 eyes (4/6 eyes; Fig. 3B).

Although the size of the *PAX77*$^{+/-}$ eyes and lens was not markedly affected at E16.5, comparison of CD1-*PAX77*$^{+/-}$ and F1-*PAX77*$^{+/-}$ fetal eyes showed that genetic background differences were already apparent by this stage of development. Lens vacuoles occurred in some of the eyes on both backgrounds (8/14). In the F1-*PAX77*$^{+/-}$ eyes, the vitreous appeared normal, but the neuroblastic layers were slightly disorganized in two of six eyes, and ingression of RPE cells was observed in the optic nerve sheath at the optic disc in some (3/6), whereas the other eyes showed a sharp boundary between the RPE and the optic nerve at the disc. Pigment cells were detected further proximally in the optic nerve sheath in one F1-*PAX77*$^{+/-}$ eye (Figs. 3H, 3I). Neural retinal and vitreous abnormalities were more prominent in the CD1-*PAX77*$^{+/-}$ eyes but RPE abnormalities were difficult to see on an albino CD1 background. Most strikingly, CD1-*PAX77*$^{+/-}$ eyes showed various degrees of retinal folding (4/8). These folds were not restricted to any portion of the retina and could be observed along the dorsal, ventral, and nasal axes (Figs. 3D, 3E). Sometimes a retinal fold was in contact with the posterior surface of the lens. The posterior lens cells were epithelial-like, suggesting that they may have been displaced from their normal anterior location. Furthermore, the CD1-*PAX77*$^{+/-}$ eyes sometimes contained a clump of retinal cells posterior to the lens (3/8 cases; Fig. 3F) similar to that seen in some adult *PAX77*$^{+/-}$ eyes. In some (3/8) of the CD1-*PAX77*$^{+/-}$ eyes, the anterior chamber angle was obstructed with cells, but this was not seen in F1-*PAX77*$^{+/-}$ eyes.

## Pax6 Expression in *PAX77*$^{+/-}$ Eyes

Previous studies have shown that Pax6 expression is increased in *PAX77*$^{+/-}$ transgenic mice on a CD1 genetic background.24,31 Immunohistochemical staining suggested that Pax6 protein levels were also elevated in *PAX77*$^{+/-}$ fetal eye tissues on a CBA/Ca inbred background (Figs. 4A, 4B). For example, Pax6 staining was stronger in the proximal RPE of E14.5 *PAX77*$^{+/-}$ eyes than in wild-type eyes, where it is downregulated.5

It was possible that the variation in severity of the PAX77 eye phenotype may reflect differences in levels of *PAX6* over-expression in ocular tissues among the mice on different genetic backgrounds. Initial investigation by Western blot on fetal eyes did not reveal clear differences in Pax6 expression between *PAX77*$^{+/-}$ mice and wild-types on any genetic background (data not shown). This is presumably because the transgenic eyes have proportionately less Pax6-expressing tissue (smaller lens and smaller thinner retina) and this would offset any increase in Pax6 level per cell in those tissues. Pax6 immunostaining levels in the E14.5 lens epithelium were therefore compared by using a modification of the

semiquantitative method described by Song et al.41 (see the Materials and Methods section), with AP2$\alpha$ expression used as an internal control. This analysis is presented in Figures 4C and 4D and more fully in Supplementary Table S1, and shows that for all three genetic backgrounds Pax6/PAX6 levels in the *PAX77*$^{+/-}$ mice were slightly (20%–29%) but significantly higher than in the wild-types. Although the severities of the abnormal PAX77 phenotypes on different genetic backgrounds increased in the rank order F1 < CBA/Ca < CD1, the rank order for normalized Pax6 staining levels in PAX77 lenses was F1 < CD1 < CBA/Ca. There was no significant difference in Pax6 protein levels between CD1-*PAX77*$^{+/-}$ and F1-*PAX77*$^{+/-}$ lenses (*t*-test: $P = 0.43$, $n = 8$), which represent the two extremes of the *PAX77* eye phenotypes. Analysis of variance confirmed that the normalized Pax6/PAX6 levels were significantly higher in *PAX77* than wild-type lenses ($P < 0.0001$) but, in contrast to the results for eye mass (discussed earlier), there was no significant interaction between genotype and genetic background for Pax6 staining ($P = 0.53$). These results do not support the hypothesis that the more severe eye abnormalities in CD1-*PAX77*$^{+/-}$ eyes reflect higher Pax6 protein levels than in F1-*PAX77*$^{+/-}$ or CBA-*PAX77*$^{+/-}$ eyes.

## Morphologic Abnormalities in Fetal *PAX77*$^{+/-}$↔Wild-Type Chimeras

Two series of E16.5 experimental *PAX77*$^{+/-}$↔wild-type chimeras were produced, each with their own set of *PAX77*$^{-/-}$↔wild-type control chimeras, as described in the Materials and Methods section. CD1A × CD1-*PAX77*$^{+/-}$ embryos were incorporated into series SCA chimeras (genotype combination of SCA experimental chimeras: *PAX77*$^{+/-}$, *Gpi1*$^{a/a}$, *Tyr*$^{c/c}$, *Tg*$^{-/-}$ ↔*PAX77*$^{-/-}$, *Gpi1*$^{b/b}$, *Tyr*$^{+/+}$, and *Tg*$^{+/-}$). CBA-*PAX77*$^{+/-}$ × BTC embryos were used for series SCB (genotype combination of SCB experimental chimeras: *PAX77*$^{+/-}$, *Gpi1*$^{b/b}$, *Tyr*$^{+/+}$, *Tg*$^{+/-}$↔*PAX77*$^{-/-}$, *Gpi1*$^{a/a}$, *Tyr*$^{c/c}$, and *Tg*$^{-/-}$). Eight experimental chimeras (seven SCA plus one SCB) and seven control chimeras (five SCA plus two SCB) were analyzed. The global *PAX77*$^{+/-}$ contribution (or *PAX77*$^{-/-}$ contribution in control chimeras) of cells from the *PAX77*$^{+/-}$ × wild-type embryo used to produce the chimera was estimated as the mean percentage of GPI1-A in several nonocular tissues for series SCA and the percentage of GPI1-B for series SCB (see the Materials and Methods section). The contributions to the lens, corneal epithelium and corneal stroma were estimated as a corrected percentage of *Tg*-negative cells for SCA chimeras and corrected percentage of *Tg*-positive cells for SCB chimeras. The contribution to the RPE was estimated as the percentage of albino cells for series SCA and the percentage of pigmented cells for SCB chimeras.

Fetal experimental *PAX77*$^{+/-}$↔wild-type chimeric eyes displayed a few morphologic abnormalities, some of which were similar to those seen in E16.5 *PAX77*$^{+/-}$ transgenic fetuses. No gross abnormalities were seen in the cornea, lens, or nasal epithelium but retinal abnormalities occurred relatively frequently (Table 2). The frequency of abnormalities correlated significantly with the global composition of the chimeras ($P = 0.032$ by Kendall's correlation), such that chimeras with high overall proportions of *PAX77*$^{+/-}$ cells tended to have more abnormalities (Table 2).

## Retinal Dysgenesis in Fetal *PAX77*$^{+/-}$↔Wild-Type Chimeras

Nine of the 16 eyes from the experimental chimeras displayed retinal dysgenesis in the form of large retinal folds similar to those in E16.5 *PAX77*$^{+/-}$ nonchimeric fetuses. These retinal overgrowths occurred only in chimeras with >40% *PAX77*$^{+/-}$ cells overall (Table 2) and were restricted to the nasal side of the retina. Spatial analysis of the distribution of wild-type and *PAX77*$^{+/-}$ cells in the dysmorphic retinas suggests both cell-autonomous effects and nonautonomous effects are involved. In some cases, the folds were composed either entirely of *PAX77*$^{+/-}$ or entirely of wild-type cells but in other cases the folds contained patches of both *PAX77*$^{+/-}$ and wild-type cells (Fig. 5A–C). The presence of both cell types in the folds

suggests that this is a non–cell-autonomous defect resulting from Pax6 overexpression or a secondary defect caused by some other affected tissue.

In some cases clusters of wild-type or *PAX77*$^{+/-}$ cells were organized into small vesicles or nests of cells of the same genotype. Figure 5D shows a small vesicle of wild-type (*Tg*$^{+/-}$) cells within a *PAX77*$^{+/-}$ domain in the retina. One possibility is that overexpression of Pax6 in *PAX77*$^{+/-}$ cells causes a cell-autonomous effect on expression of cell surface adhesion molecules. This could cause reduced cell mixing, resulting in the formation of coherent clones of daughter cells and/or sorting-out of neighboring wild-type and *PAX77*$^{+/-}$ cells.

A small ectopic ball of retinal cells occurred between the lens and nasal side of the retina in one eye of *PAX77*$^{+/-}$↔wild-type experimental chimera SCA12 (Fig. 5E). This chimera had the highest global proportion of *PAX77*$^{+/-}$ cells (87%) and the ectopic ball of cells was also mostly *PAX77*$^{+/-}$, but it did contain a few *Tg*-positive wild-type cells. The presence of both cell types suggests that this is a non–cell-autonomous defect caused by overexpression of Pax6 in *PAX77*$^{+/-}$ tissues but further examples are needed to determine whether *PAX77*$^{+/-}$ cells are overrepresented. Similar ectopic balls of cells occurred in some nonchimeric, adult, and fetal CD1-*PAX77*$^{+/-}$ eyes (Figs. 2T, 3F) but not in the wild-type eyes.

## Sorting-Out of *PAX77*$^{+/-}$ and Wild-Type Cells in Other Ocular Tissues in Chimeras

In the anterior segment of control chimeras, *Tg*-positive and -negative cells contributed freely to all tissues and were fairly evenly distributed (Fig. 5F). In contrast, cells in the developing ciliary bodies were segregated into patches of like genotype in 6 of 16 eyes from experimental *PAX77*$^{+/-}$↔wild-type chimeras (Figs. 5G–I; Table 2). In these cases, the near-distal domain of the neural retina that is fated to become the ciliary body was largely composed of *Tg*-negative *PAX77*$^{+/-}$ cells, but had balls or buds of *Tg*-positive wild-type cells projecting from the inner edge, facing the lens (Figs. 5H, 5I). This observation shows that *PAX77*$^{+/-}$ cells can contribute to the early stages of ciliary body specification and suggests that Pax6 dosage could modulate cell surface adhesion properties in a cell-autonomous way that leads to reduced cell mixing and sorting-out of the cells in chimeras.

Cell segregation in the iris pigment epithelium (IPE) occurred in 6 of 16 eyes from the experimental chimeras (Table 2) with *PAX77*$^{+/-}$ cells ectopically bulging from a largely wild-type iris pigment epithelium (Fig. 5G). Balls of *PAX77*$^{+/-}$ cells were also occasionally observed in the trabecular meshwork of a few of these eyes, which may indicate segregation on the basis of Pax6 dosage in this tissue too (Fig. 5J). However, it is possible that these were balls of dislodged *PAX77*$^{+/-}$ IPE cells, for which the link to the rest of the IPE had been lost or was not visible.

## Segregation of *PAX77*$^{+/-}$ and Wild-Type Cells in Nasal Tissues of Chimeras

A clump of serous gland tubules, on each side of the nasal region, expresses Pax6 (Fig. 5K) and is connected to and forms part of the nasal epithelia. Frequently, in the *PAX77*$^{+/-}$↔wild-type chimeras, *PAX77*$^{-/-}$ cells were segregated to the smaller peripheral tubules, whereas the larger central tubules were very predominantly *PAX77*$^{+/-}$ (Fig 5L). This segregation is incomplete and could be partly a consequence of clonal growth of the tubules. However, it occurred much more frequently in experimental *PAX77*$^{+/-}$↔wild-type chimeras (11/16) than control chimeras (1/14), and this difference was highly significant by Fisher's exact test ($P = 0.0008$). If the two genetically distinct cell populations showed a greater tendency to clump together in larger patches during development of experimental chimeras than in wild-type chimeras, it may cause tubules to develop from cells of a single genotype more frequently.

### Abnormal Intrusion of *PAX77*$^{+/-}$ Cells into the Optic Nerve Sheath in Chimeras

Coherent groups of RPE cells intruded into the sheath of the optic nerve in most (14/16) of the eyes of experimental *PAX77*$^{-/-}$↔wild-type chimeras (Figs. 5M–O; Table 2). This involved both *PAX77*$^{+/-}$ and *PAX77*$^{-/-}$ RPE cells, implying that it was not a cell autonomous effect. Although single RPE cells also sometimes occurred in the distal optic nerve sheath in control *PAX77*$^{-/-}$↔wild-type chimeras, groups of RPE cells were never seen. This ingression of RPE cells into the optic nerve sheath was also noted in nonchimeric fetal *PAX77*$^{+/-}$ eyes (Figs. 3H, 3I).

### Elevated Contributions of *PAX77*$^{+/-}$ Cells to the Lens Epithelium and RPE in Fetal Chimeras

The analysis of chimeras discussed earlier indicates that *PAX77*$^{+/-}$ cells contributed to all ocular and nasal tissues that were examined in the experimental *PAX77*$^{+/-}$↔wild-type chimeras in series SCA and SCB. The qualitative observations showed that, unlike *Pax6*$^{+/-}$ cells,14 *PAX77*$^{+/-}$ cells were not excluded from the lens epithelium of chimeras by E16.5. Quantitative analysis of four eye tissues was undertaken to test whether *PAX77*$^{+/-}$ cells were at least depleted from the lens epithelium of chimeras.

For *PAX77*$^{+/-}$↔wild-type experimental chimeras in series SCA the *PAX77*$^{+/-}$ contributions to specific eye tissues were estimated from the observed corrected percentage of *Tg*-negative cells (or observed percentage of albino cells for the RPE). This was divided by the contribution expected from the global estimate of the percentage of GPI1-A. Low observed/expected (corrected percentage of *Tg*-negative/percentage of GPI1-A) ratios suggest underrepresentation of *PAX77*$^{+/-}$ cells in the specific tissue. Observed/expected ratios for four eye tissues from experimental chimeras in series SCA were compared to the equivalent ratios for the control chimeras. The results (Fig. 6) showed that *PAX77*$^{+/-}$ cells were not underrepresented in the lens epithelium but were slightly but significantly overrepresented. The mean observed/expected contribution ratio for the lens epithelia in the 14 eyes from experimental SCA chimeras was 1.41 ± 0.14 versus 0.98 ± 0.08 for the 10 control chimeric eyes ($P = 0.03$). *PAX77*$^{+/-}$ cells also showed a small but significant overrepresentation in the RPE (1.52 ± 0.19 vs. 1.03 ± 0.05; $P = 0.04$). *PAX77*$^{+/-}$ cells were neither significantly overrepresented nor underrepresented in the corneal epithelium and corneal stroma. Addition of results for the SCB chimeras made no difference in the conclusions (Fig. 6B). For chimeras in series SCB, observed contributions were estimated as the corrected percentage of *Tg*-positive cells or observed percentage of pigmented RPE cells and the expected contribution was estimated as the percentage of GPI1-B. These quantitative results suggest that elevated Pax6 expression in *PAX77*$^{+/-}$ cells has a cell-autonomous effect in both the lens epithelium and RPE although, in each case, the effect is small.

## Discussion

### Genetic Background and Stochastic Effects on the *PAX77*$^{+/-}$ Phenotype

The original report of elevated Pax6 expression in *PAX77*$^{+/-}$ transgenic mice on a wild-type (*Pax6*$^{+/+}$) background24 described a variable phenotype that included microphthalmia and other eye abnormalities. We found a similar range of abnormalities but showed that the *PAX77*$^{+/-}$ phenotype is critically dependent on the genetic background. Penetrance and expressivity of different phenotypes increased in the order F1-*PAX77*$^{+/-}$ < CBA-*PAX77*$^{+/-}$ < CD1-*PAX77*$^{+/-}$. Eye mass correlated well with the severity of the morphologic abnormalities and provided a sensitive quantitative measure of both the severity and the variability of the phenotype. Semiquantitative analysis of Pax6 protein levels provided no evidence that the differences in *PAX77* eye phenotypes on different genetic backgrounds were caused by differences in Pax6 protein levels in *PAX77*$^{+/-}$ eyes.

*PAX77*$^{+/-}$ eye size was originally described as varying from almost normal to severe microphthalmia.24 but when we obtained CD1-*PAX77*$^{+/-}$ mice in 2001, the phenotype was very severe, and no eyes were nearly normal in size. This apparent increase in severity with time may reflect selection for a permissive genetic background, that produces a more consistently severe phenotype, in the outbred CD1 strain as a byproduct of choosing mice with an unambiguous phenotype for breeding. Genetic background affects the penetrance of some homozygous *Pax6*$^{-/-}$ phenotypes12 and may also explain the greater range of abnormal eye phenotypes reported for heterozygous *Pax6*$^{Sey/+}$ mice on a CD1 genetic background18 than reported previously for *Pax6*$^{Sey/+}$ heterozygotes. This suggests that the gene pool of the outbred CD1 strain contains alleles of modifier genes that influence the expressivity and penetrance of various abnormal ocular phenotypes in *Pax6*$^{Sey/+}$ or *PAX77*$^{+/-}$ mice. Selection for a severe phenotype would then select for combinations of modifier genes that were permissive for many abnormal *PAX77*$^{+/-}$ phenotypes.

Within-mouse variation in eye mass was greater on inbred CBA/Ca and outbred CD1 genetic backgrounds than the F1 hybrid background. Genetic differences do not cause this variation directly but could affect the occurrence of stochastic variation. Eye size is, therefore, likely to be affected by three factors: *PAX77*$^{+/-}$ genotype, genetic background, and stochastic variation. This finding highlights the importance of standardizing the genetic background of mice when comparing the phenotypic effects of different mutants or transgenes.

## Differences between Phenotypes Caused by High and Low Pax6 Expression

Although both *Pax6*$^{+/-}$ mice with low Pax6 levels and *PAX77*$^{+/-}$ mice with elevated Pax6 expression cause microphthalmia and an overlapping spectrum of other eye abnormalities, there are significant differences in the abnormalities produced by the two genotypes (Table 3). Abnormalities of CBA-*PAX77*$^{+/-}$ corneas are reported in more detail elsewhere.42

## Possible Mechanisms Underlying Effects of Pax6 Overexpression in *PAX77*$^{+/-}$ Tissues

Absence of Pax6 may either reduce or enhance proliferation, depending on the tissue,25 and the same may be true of overexpression. Indeed, we found *PAX77*$^{+/-}$ cells to be overrepresented in the RPE and lens epithelium, whereas *PAX77*$^{+/-}$ cells were depleted in some regions of the brain.31 Pax6 overexpression slowed proliferation in rabbit corneal epithelial cells45,46 but increased retinal cell proliferation.47 Reduced cell proliferation may affect eye size and/or corneal diameter. Increased cell proliferation could contribute to the retinal dysplasia in *PAX77*$^{+/-}$ eyes and provide a competitive advantage for *PAX77*$^{+/-}$ cells in the lens epithelium and/or RPE of *PAX77*$^{+/-}$↔wild-type chimeras, where *PAX77*$^{+/-}$ cells were enriched.

Some *PAX77*$^{+/-}$ eye abnormalities may be due to a disruption of the ratio between Pax6 and other factors, with which it interacts to control gene expression.48 However, the extent to which Pax6 protein levels are elevated in each eye tissue is difficult to predict. According to Schedl et al.,24 *PAX77*$^{+/-}$ mice have five to six copies of the human *PAX6* gene and express the equivalent of 5 to 8 copies of human *PAX6* mRNA in both severely and mildly affected eyes. The increase in Pax6 levels in fetal *PAX77*$^{+/-}$ lenses was less than predicted from the gene copy numbers. This finding is consistent with those in studies of fetal brain31 and adult cornea42 and probably reflects negative autoregulation of Pax6.31

Alternative splicing49-52 and promoter usage53,54 to produce different isoforms causes another complication. Pax6(5a) contains 14 more amino acids than the predominant Pax6 isoform, which disrupts its ability to bind to DNA. Overexpression of either the Pax6 or Pax6(5a) isoform in different systems has highlighted effects of specific isoforms on gene

expression, cell biology, and eye development.55-61 The ratio of Pax6 to Pax6(5a) protein isoforms differs in wild-type and *PAX77*$^{+/-}$ brains.31 If the isoform ratio varies with *Pax6* genotype and among different eye tissues, the consequences for eye development would be difficult to predict.

## Cell-Autonomous Effect of Pax6 Overexpression in the *PAX77*$^{+/-}$ Lens Epithelium

*PAX77*$^{+/-}$ cells showed a small but significant overrepresentation in the lens epithelium, implying that the *PAX77*$^{+/-}$ genotype has a cell-autonomous effect. The type of effect differs from that seen in *Pax6*$^{+/-}$↔wild-type chimeras where *Pax6*$^{+/-}$ cells were excluded from the lens epithelium by E16.5.14 The reciprocal cell-autonomous effects of *Pax6*$^{+/-}$ and *PAX77*$^{+/-}$ in chimeras suggest that the probability of lens epithelial cell survival depends on the level of Pax6 expression. For example, an effect of Pax6 level on differential cell adhesion may explain the chimera observations if cell adhesiveness increased in the order *Pax6*$^{+/-}$ < wild-type < *PAX77*$^{+/-}$. If the two populations of lens epithelial cells in chimeras tended to sort out so that less adhesive cells surrounded more adhesive cells,62,63 the less adhesive cells would preferentially move to the periphery and differentiate into fiber cells.

A more direct effect of Pax6 expression on epithelial cell proliferation and/or lens fiber cell differentiation is probably also involved. Fiber cell differentiation is characterized by a decline in Pax6 levels and upregulation of the transcription factor cMaf, which regulates expression of lens crystallins.6,64-67 Overexpression of Pax6 in the lenses of transgenic mice causes low levels of cMaf,58 incomplete fiber elongation, and cataracts. Thus, high Pax6 levels in *PAX77*$^{+/-}$ lens epithelial cells could impair or delay their differentiation into fiber cells and explain both the occurrence of apparently undifferentiated lens epithelial cells among lens fibers in *PAX77*$^{+/-}$ lenses (Fig. 2Q) and the enrichment for *PAX77*$^{+/-}$ cells in the *PAX77*$^{+/-}$↔wild-type lens epithelium. The depletion of *Pax6*$^{+/-}$ cells from the lens epithelium of *Pax6*$^{+/-}$↔wild-type chimeras14 could similarly be explained by low Pax6 levels causing early upregulation of cMaf and precocious differentiation of *Pax6*$^{+/-}$ lens epithelial cells into fiber cells.

## Cell-Autonomous and Nonautonomous Effects of Pax6 in Other *PAX77*$^{+/-}$ Eye Tissues

Cell-autonomous effects were implicated by the overrepresentation of *PAX77*$^{+/-}$ cells in the RPE and abnormal cell mixing in several other tissues. Normally, Pax6 expression is downregulated in the RPE during fetal development5 but downregulation appears to be delayed in *PAX77*$^{+/-}$ eyes (Figs. 4A, 4B). This delay might increase proliferation of *PAX77*$^{+/-}$ RPE cells, resulting in their overrepresentation in chimeras. *PAX77*$^{+/-}$ and wild-type cells failed to mix normally in several tissues of *PAX77*$^{+/-}$↔wild-type chimeras and tended to sort out or form vesicles or buds of cells of a single genotype, which were not seen in control chimeras. This observation implies that differences in Pax6 levels in *PAX77*$^{+/-}$ and wild-type cells act cell autonomously to reduce cell mixing between cells of different genotypes, probably by altering expression of cell surface adhesion molecules.

Intrusion of RPE cells into the optic nerve sheath and folding of the neural retina seem to be nonautonomous effects because both wild-type and *PAX77*$^{+/-}$ cells were involved. Intrusion of RPE cells into the sheath of the optic nerve has been reported previously in *Pax2*$^{-/-}$ embryos68 and the position of the optic cup/optic stalk boundary depends on expression of Pax2 and Pax6, which negatively regulate each other. Overexpression of Pax6 or a delay in its downregulation could cause the optic cup/optic stalk boundary to be displaced proximally. Convoluted overgrowth of retinal tissue occurs in the absence of a lens6,26,30,69-71 and in the presence of a small lens in the *aphakia* mutant.72 Thus, the retinal overgrowth in fetal *PAX77*$^{+/-}$↔wild-type chimeras could be secondary to a lens

abnormality, but analysis of later stage chimeras may be necessary to demonstrate any correlation.

### Differences between *Pax6*$^{+/-}$↔Wild-Type and *PAX77*$^{+/-}$↔Wild-Type Chimeras

Overall, *PAX77*$^{+/-}$↔wild-type chimeras were less severely affected than homozygous *Pax6*$^{-/-}$↔wild-type chimeras26-28 but had more abnormalities than *Pax6*$^{+/-}$↔wild-type chimeras14 (Table 4). The only effect seen in our *Pax6*$^{+/-}$↔wild-type chimeras was a cell-autonomous exclusion of *Pax6*$^{+/-}$ cells in the lens epithelium by E16.5, producing an almost entirely wild-type lens. As suggested previously,14 normalization of the lens genotype may have secondary effects elsewhere in the eye so that no morphologic abnormalities or nonautonomous effects of the *Pax6*$^{+/-}$ genotype were apparent. In contrast, *PAX77*$^{+/-}$ cells were overrepresented in the lens epithelia of *PAX77*$^{+/-}$↔wild-type chimeras, and these chimeras showed several morphologic abnormalities as well as other cell-autonomous and nonautonomous effects (Table 4).

## Supplementary Material

Refer to Web version on PubMed Central for supplementary material.

## Acknowledgments

The authors thank Veronica van Heyningen for providing a founder stock of PAX77 mice; Jean Flockhart, Ailsa Travers, Julie Thomson, and Matthew Sharp for assistance with chimera production; Jane Quinn and Michael Molinek for technical advice; Denis Doogan, Maureen Ross and Mark Fisken for expert mouse husbandry; Rob Elton for statistical advice; and David Price for helpful discussion.

Supported by Wellcome Trust Grant 065035 (JDW).

## References

1. Cvekl A, Tamm ER. Anterior eye development and ocular mesenchyme: new insights from mouse models and human diseases. Bioessays. 2004; 26:374–386. [PubMed: 15057935]
2. Hill RE, Favor J, Hogan BLM, et al. Mouse small eye results from mutations in a paired-like homeobox-containing gene. Nature. 1991; 354:522–525. [PubMed: 1684639]
3. Ton CCT, Hirvonen H, Miwa H, et al. Positional cloning and characterization of a paired box-containing and homeobox-containing gene from the aniridia region. Cell. 1991; 67:1059–1074. [PubMed: 1684738]
4. Walther C, Gruss P. *Pax-6*, a murine paired box gene, is expressed in the developing CNS. Development. 1991; 113:1435–1449. [PubMed: 1687460]
5. Grindley JC, Davidson DR, Hill RE. The role of *Pax-6* in eye and nasal development. Development. 1995; 121:1433–1442. [PubMed: 7789273]
6. Ashery-Padan R, Marquardt T, Zhou XL, Gruss P. Pax6 activity in the lens primordium is required for lens formation and for correct placement of a single retina in the eye. Genes Dev. 2000; 14:2701–2711. [PubMed: 11069887]
7. Koroma BM, Yang JM, Sundin OH. The Pax-6 homeobox gene is expressed throughout the corneal and conjunctival epithelia. Invest Ophthalmol Vis Sci. 1997; 38:108–120. [PubMed: 9008636]
8. Macdonald R, Wilson SW. Distribution of Pax6 protein during eye development suggests discrete roles in proliferative and differentiated visual cells. Dev Genes Evol. 1997; 206:363–369.
9. Hogan BM, Horsburgh G, Cohen J, Hetherington CM, Fisher G, Lyon MF. *Small eyes (Sey)*: a homozygous lethal mutation on chromosome 2 which affects the differentiation of both lens and nasal placodes in the mouse. J Embryol Exp Morphol. 1986; 97:95–110. [PubMed: 3794606]
10. Hogan BLM, Hirst EMA, Horsburgh G, Hetherington CM. *Small eye (Sey)*: a mouse model for the genetic analysis of craniofacial abnormalities. Development. 1988; 103(suppl):115–119. [PubMed: 3250848]

11. Schmahl W, Knoedlseder M, Favor J, Davidson D. Defects in neuronal migration and the pathogenesis of cortical malformations are associated with Small eye (Sey) in the mouse, a point mutation of the Pax-6-locus. Acta Neuropathol. 1993; 86:126–135. [PubMed: 8213068]
12. Quinn JC, West JD, Kaufman MH. Genetic background effects on dental and other craniofacial abnormalities in homozygous small eye (*Pax6*$^{Sey}$/*Pax6*$^{Sey}$) mice. Anat Embryol. 1997; 196:311–321. [PubMed: 9363853]
13. Glaser T, Jepeal L, Edwards JG, Young SR, Favor J, Maas R. PAX6 gene dosage effects in a family with congenital cataracts, aniridia, anophthalmia and central nervous system defects. Nat Genet. 1994; 7:463–471. (published correction in *Nat Genet*. 1995;8:203). [PubMed: 7951315]
14. Collinson JM, Quinn JC, Buchanan MA, et al. Primary defects in the lens underlie complex anterior segment abnormalities of the *Pax6* heterozygous eye. Proc Nat Acad Sci USA. 2001; 98:9688–9693. [PubMed: 11481423]
15. van Raamsdonk CD, Tilghman SM. Dosage requirement and allelic expression of *PAX6* during lens placode formation. Development. 2000; 127:5439–5448. [PubMed: 11076764]
16. Ramaesh T, Collinson JM, Ramaesh K, Kaufman MH, West JD, Dhillon B. Corneal abnormalities in *Pax6*$^{+/-}$ small eye mice mimic human aniridia-related keratopathy. Invest Ophthalmol Vis Sci. 2003; 44:1871–1878. [PubMed: 12714618]
17. Baulmann DC, Ohlmann A, Flugel-Koch C, Goswami S, Cvekl A, Tamm ER. *Pax6* heterozygous eyes show defects in chamber angle differentiation that are associated with a wide spectrum of other anterior eye segment abnormalities. Mech Dev. 2002; 118:3–17. [PubMed: 12351165]
18. Kanakubo S, Nomura T, Yamamura KI, Miyazaki JI, Tamai M, Osumi N. Abnormal migration and distribution of neural crest cells in Pax6 heterozygous mutant eye, a model for human eye diseases. Genes Cells. 2006; 11:919–933. [PubMed: 16866875]
19. Davis J, Duncan MK, Robison WG, Piatigorsky J. Requirement for Pax6 in corneal morphogenesis: a role in adhesion. J Cell Sci. 2003; 116:2157–2167. [PubMed: 12692153]
20. Hanson IM, Fletcher JM, Jordan T, et al. Mutations at the PAX6 locus are found in heterogeneous anterior segment malformations including Peters' anomaly. Nat Genet. 1994; 6:168–173. [PubMed: 8162071]
21. Hanson I, Churchill A, Love J, et al. Missense mutations in the most ancient residues of the *PAX6* paired domain underlie a spectrum of human congenital eye malformations. Hum Mol Genet. 1999; 8:165–172. [PubMed: 9931324]
22. Nishida K, Kinoshita S, Ohashi Y, Kuwayama Y, Yamamoto S. Ocular surface abnormalities in aniridia. Am J Ophthalmol. 1995; 120:368–375. [PubMed: 7661209]
23. Aalfs CM, Fantes JA, WennigerPrick L, et al. Tandem duplication of 11p12–p13 in a child with borderline development delay and eye abnormalities: dose effect of the PAX6 gene product? Am J Med Genet. 1997; 73:267–271. [PubMed: 9415682]
24. Schedl A, Ross A, Lee M, et al. Influence of *Pax6* gene dosage on development: overexpression causes severe eye abnormalities. Cell. 1996; 86:71–82. [PubMed: 8689689]
25. Simpson TI, Price DJ. Pax6: a pleiotropic player in development. Bioessays. 2002; 24:1041–1051. [PubMed: 12386935]
26. Quinn JC, West JD, Hill RE. Multiple functions for *Pax6* in mouse eye and nasal development. Genes Dev. 1996; 10:435–446. [PubMed: 8600027]
27. Collinson JM, Hill RE, West JD. Different roles for *Pax6* in the optic vesicle and facial epithelium mediate early morphogenesis of the murine eye. Development. 2000; 127:945–956. [PubMed: 10662634]
28. Collinson JM, Quinn JC, Hill RE, West JD. The roles of *Pax6* in the cornea, retina, and olfactory epithelium of the developing mouse embryo. Dev Biol. 2003; 255:303–312. [PubMed: 12648492]
29. Davis-Silberman N, Kalich T, Oron-Karni V, et al. Genetic dissection of Pax6 dosage requirements in the developing mouse eye. Hum Mol Genet. 2005; 14:2265–2276. [PubMed: 15987699]
30. Li S, Goldowitz D, Swanson DJ. The requirement of Pax6 for postnatal eye development: evidence from experimental mouse chimeras. Invest Ophthalmol Vis Sci. 2007; 48:3292–3300. [PubMed: 17591901]
31. Manuel M, Georgala PA, Carr CB, et al. Controlled overexpression of Pax6 in vivo negatively auto-regulates the *Pax6* locus, causing cell-autonomous defects of late cortical progenitor

proliferation with little effect on cortical arealization. Development. 2007; 134:545–555. [PubMed: 17202185]

32. West JD, Flockhart JH. Genotypically unbalanced diploid↔ diploid foetal mouse chimaeras: possible relevance to human confined mosaicism. Genet Res. 1994; 63:87–99. [PubMed: 8026741]
33. Tarkowski AK. Mouse chimaeras developed from fused eggs. Nature. 1961; 190:857–860. [PubMed: 13775333]
34. Lo CW, Coulling M, Kirby C. Tracking of mouse cell lineage using microinjected DNA sequences: analysis using genomic Southern blotting and tissue-section in situ hybridizations. Differentiation. 1987; 35:37–44. [PubMed: 3428512]
35. Keighren M, West JD. Analysis of cell ploidy in histological sections of mouse tissues by DNA-DNA in situ hybridization with digoxygenin labelled probes. Histochem J. 1993; 25:30–44. [PubMed: 8432662]
36. Whittingham DG. Culture of mouse ova. J Reprod Fert. 1971; 14(suppl):7–21.
37. Lawitts, JA.; Biggers, JD. Culture of preimplantation embryos. In: Wasserman, PM.; DePamphilis, ML., editors. Guide to Techniques in Mouse Development: Methods in Enzymology. Academic Press Inc; San Diego: 1993. p. 153-164.
38. Erbach GT, Lawitts JA, Papaioannou VE, Biggers JD. Differential growth of the mouse preimplantation embryo in chemically defined media. Biol Reprod. 1994; 50:1027–1033. [PubMed: 8025158]
39. Quinn P, Barros C, Whittingham DG. Preservation of hamster oocytes to assay the fertilizing capacity of human spermatozoa. J Reprod Fert. 1982; 66:161–168.
40. Summers MC, Bhatnagar PR, Lawitts JA, Biggers JD. Fertilization in vitro of mouse ova from inbred and outbred strains: complete preimplantation embryo development in glucose-supplemented KSOM. Biol Reprod. 1995; 53:431–437. [PubMed: 7492697]
41. Song N, Schwab KR, Patterson LT, et al. Pygopus 2 has a crucial, Wnt pathway-independent function in lens induction. Development. 2007; 134:1873–1885. [PubMed: 17428831]
42. Dorà N, Ou J, Kucerova R, Parisi I, West JD, Collinson JM. PAX6 dosage effects on corneal development, growth and wound healing. Dev Dyn. 2008; 237:1295–1306. [PubMed: 18386822]
43. Clayton RM. Problems of differentiation in the vertebrate lens. Curr Top Dev Biol. 1970; 5:115–180. [PubMed: 4118743]
44. Roberts RC. Small eyes-a new dominant eye mutant in the mouse. Genet Res. 1967; 9:121–122.
45. Li T, Lu L. Epidermal growth factor-induced proliferation requires down-regulation of Pax6 in corneal epithelial cells. J Biol Chem. 2005; 280:12988–12995. [PubMed: 15659382]
46. Ouyang J, Shen YC, Yeh LK, et al. *Pax6* overexpression suppresses cell proliferation and retards the cell cycle in corneal epithelial cells. Invest Ophthalmol Vis Sci. 2006; 47:2397–2407. [PubMed: 16723449]
47. Azuma N, Tadokoro K, Asaka A, et al. The Pax6 isoform bearing an alternative spliced exon promotes the development of the neural retinal structure. Hum Mol Genet. 2005; 14:735–745. [PubMed: 15677484]
48. Chauhan BK, Yang Y, Cveklova K, Cvekl A. Functional interactions between alternatively spliced forms of Pax6 in crystallin gene regulation and in haploinsufficiency. Nuc Acid Res. 2004; 32:1696–1709.
49. Epstein JA, Glaser T, Cai JX, Jepeal L, Walton DS, Maas RL. Two independent and interactive DNA-binding subdomains of the Pax6 paired domain are regulated by alternative splicing. Genes Dev. 1994; 8:2022–2034. [PubMed: 7958875]
50. Richardson J, Cvekl A, Wistow G. *Pax-6* is essential for lens-specific expression of ζ-crystallin. Proc Natl Acad Sci USA. 1995; 92:4676–4680. [PubMed: 7753863]
51. Jaworski C, Sperbeck S, Graham C, Wistow G. Alternative splicing of Pax6 in bovine eye and evolutionary conservation of intron sequences. Biochem Biophys Res Commun. 1997; 240:196–202. [PubMed: 9367909]
52. Kozmik Z, Czerny T, Busslinger M. Alternatively spliced insertions in the paired domain restrict the DNA sequence specificity of Pax6 and Pax8. EMBO J. 1997; 16:6793–6803. [PubMed: 9362493]

53. Kim J, Lauderdale JD. Analysis of Pax6 expression using a BAC transgene reveals the presence of a paired-less isoform of Pax6 in the eye and olfactory bulb. Dev Biol. 2006; 292:486–505. [PubMed: 16464444]
54. Kleinjan DA, Seawright A, Mella S, et al. Long-range downstream enhancers are essential for Pax6 expression. Dev Biol. 2006; 299:563–581. [PubMed: 17014839]
55. Chauhan BK, Reed NA, Yang Y, et al. A comparative cDNA microarray analysis reveals a spectrum of genes regulated by Pax6 in mouse lens. Genes Cells. 2002; 7:1267–1283. [PubMed: 12485166]
56. Chauhan BK, Reed NA, Zhang WJ, Duncan MK, Kilimann MW, Cvekl A. Identification of genes downstream of Pax6 in the mouse lens using cDNA microarrays. J Biol Chem. 2002; 277:11539–11548. [PubMed: 11790784]
57. Duncan MK, Kozmik Z, Cveklova K, Piatigorsky J, Cvekl A. Overexpression of PAX6(5a) in lens fiber cells results in cataract and upregulation of $\alpha 5\beta 1$ integrin expression. J Cell Sci. 2000; 113:3173–3185. [PubMed: 10954416]
58. Duncan MK, Xie LK, David LL, et al. Ectopic Pax6 expression disturbs lens fiber cell differentiation. Invest Ophthalmol Vis Sci. 2004; 45:3589–3598. [PubMed: 15452066]
59. Leconte L, Lecoin L, Martin P, Saule S. Pax6 interacts with cVax and Tbx5 to establish the dorsoventral boundary of the developing eye. J Biol Chem. 2004; 279:47272–47277. [PubMed: 15322073]
60. Duncan MK, Haynes JI, Cvekl A, Piatigorsky J. Dual roles for Pax-6: a transcriptional repressor of lens fiber cell-specific $\beta$-crystallin genes. Mol Cell Biol. 1998; 18:5579–5586. [PubMed: 9710641]
61. Kralova J, Czerny T, Spanielova H, Ratajova V, Kozmik Z. Complex regulatory element within the $\gamma$E- and $\gamma$F-crystallin enhancers mediates Pax6 regulation and is required for induction by retinoic acid. Gene. 2002; 286:271–282. [PubMed: 11943482]
62. Steinberg MS. Does differential adhesion govern self assembly processes in histogenesis?—equilibrium configurations and the emergence of a hierarchy among populations of embryonic cells. J Exp Zool. 1970; 173:395–434. [PubMed: 5429514]
63. Steinberg MS, Takeichi M. Experimental specification of cell sorting, tissue spreading, and specific spatial patterning by quantitative differences in cadherin expression. Proc Natl Acad Sci USA. 1994; 91:206–209. [PubMed: 8278366]
64. Kawauchi S, Takahashi S, Nakajima O, et al. Regulation of lens fiber cell differentiation by transcription factor c-Maf. J Biol Chem. 1999; 274:19254–19260. [PubMed: 10383433]
65. Wigle JT, Chowdhury K, Gruss P, Oliver G. Prox1 function is crucial for mouse lens-fibre elongation. Nat Genet. 1999; 21:318–322. [PubMed: 10080188]
66. Sakai M, Serria MS, Ikeda H, Yoshida K, Imaki J, Nishi S. Regulation of c-maf gene expression by Pax6 in cultured cells. Nuc Acid Res. 2001; 29:1228–1237.
67. Ring BZ, Cordes SP, Overbeek PA, Barsh GS. Regulation of mouse lens fiber cell development and differentiation by the Maf gene. Development. 2000; 127:307–317. [PubMed: 10603348]
68. Schwarz M, Cecconi F, Bernier G, et al. Spatial specification of mammalian eye territories by reciprocal transcriptional repression of Pax2 and Pax6. Development. 2000; 127:4325–4334. [PubMed: 11003833]
69. Breitman ML, Clapoff S, Rossant J, et al. Genetic ablation: targeted expression of a toxin genes causes microphthalmia in transgenic mice. Science. 1987; 238:1563–1565. [PubMed: 3685993]
70. Kaur S, Key B, Stock J, McNeish JD, Akeson R, Potter SS. Targeted ablation of alpha-crystallin-synthesizing cells produces lens-deficient eyes in transgenic mice. Development. 1989; 105:613–619. [PubMed: 2612368]
71. Harrington L, Klintworth GK, Secor TE, Breitman ML. Developmental analysis of ocular morphogenesis in $\alpha$A-crystallin/diphtheria toxin transgenic mice undergoing ablation of the lens. Dev Biol. 1991; 148:508–516. [PubMed: 1743399]
72. Zwaan J, Webster EH. Localisation of keratin in the cells of the cornea in aphakia and normal mouse. Exp Eye Res. 1985; 40:127–133. [PubMed: 2579838]

Europe PMC Funders Author Manuscripts

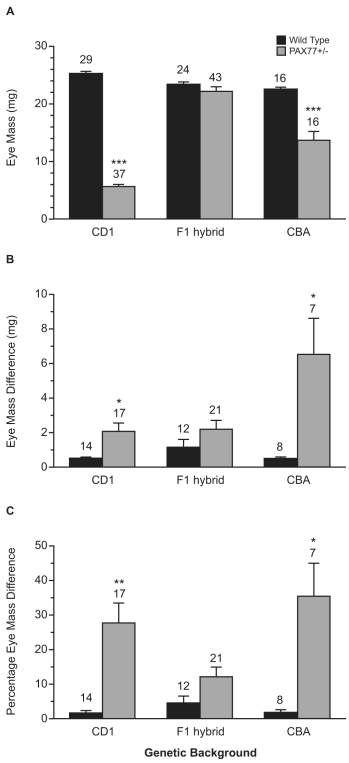


**Figure 1.**

Effect of elevated Pax6 expression and genetic background on eye size and variation in eye size within mice. (**A**) Mean mass (±SEM) of wild-type and *PAX77*$^{+/-}$ eyes from 12-week-old mice on three different genetic backgrounds. (**B**) Mean difference in mass between left and right eyes (±SEM) for the six groups. (**C**) The percentage eye mass difference, calculated as [1 − (smaller eye mass/larger eye mass)] ×100%, for the six groups. The numbers above each bar in (**A**) are the number of eyes and in (**B, C**) the number of pairs of eyes. (Only mice with two undamaged eyes were included in **B, C**.) *$P < 0.01$; **$P < 0.001$ ; ***$P < 0.0001$ for comparison between *PAX77*$^{+/-}$ and wild-type eyes on the same genetic background (*t*-tests).

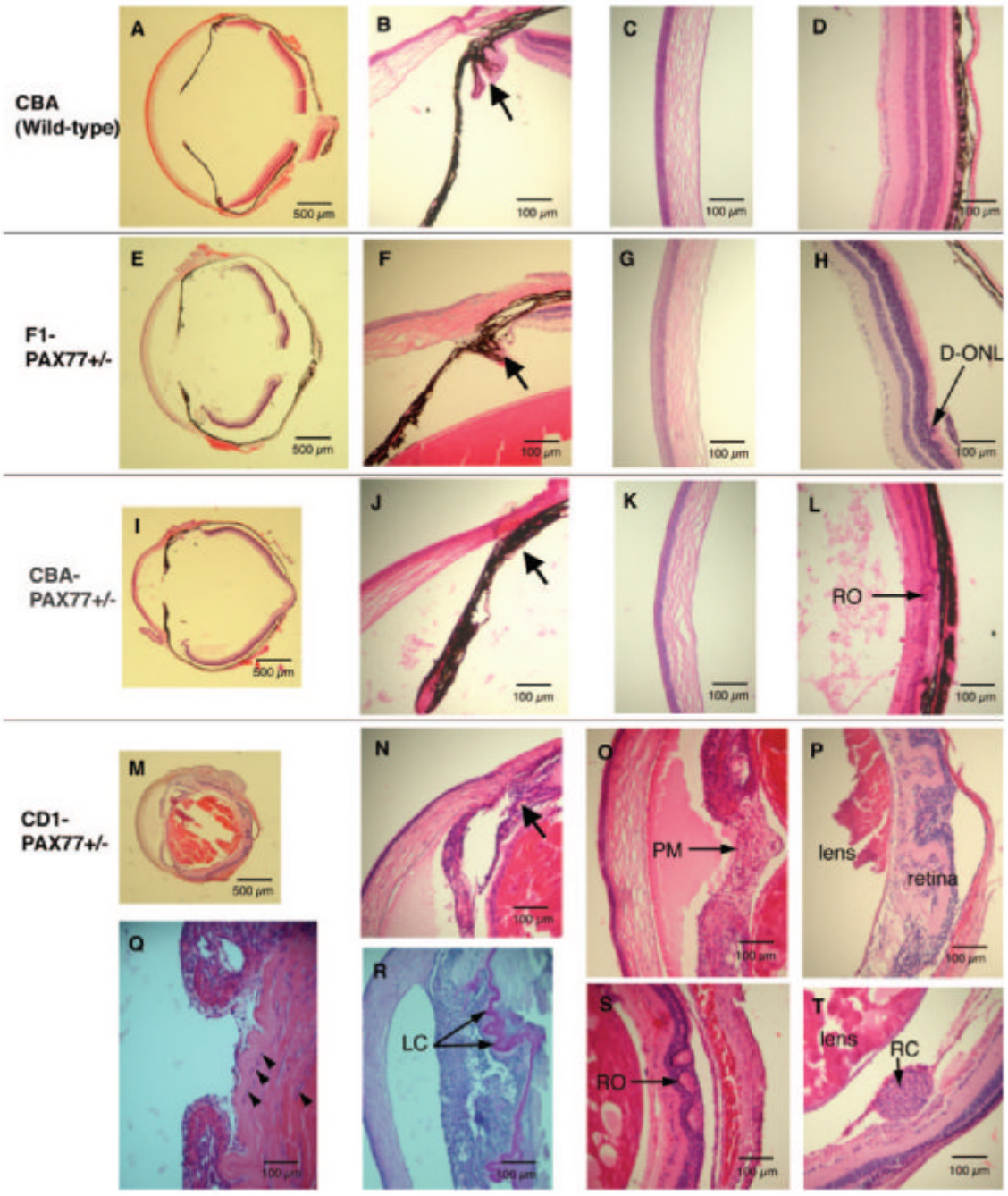


**Figure 2.**

Histologic comparison of adult *PAX77*$^{+/-}$ eye abnormalities (12 weeks) on three different genetic backgrounds. (**A–D**) Wild-type CBA eyes showing normal features: (**A**) whole eye with lens removed, (**B**) ciliary body (*arrow*) and iris, (**C**) cornea, (**D**) retina. (**E–H**) F1-*PAX77*$^{+/-}$ eyes: (**E**) normal sized eye with reduced corneal diameter and flattened cystic irides (lens removed); (**F**) abnormal ciliary body and cystic iris (*arrow*; lens present); (**G**) normal cornea (**H**) minor abnormality in ONL of neural retina (*arrow*) (neural retina has separated from RPE during processing). (**I–L**) CBA-*PAX77*$^{+/-}$ eyes: (**I**) small eye with proportionately reduced corneal diameter (lens removed), (**J**) absent ciliary body and

thickened, cystic iris (*arrow*), (**K**) cornea with normal epithelium, (**L**) eosinophilic material in the vitreous and thin retina with rosettes (RO, *arrow*). (**M–T**) Albino CD1-*PAX77*$^{+/-}$ eyes: (**M**) severely microphthalmic and disorganized eye (lens intact), (**N**) absent ciliary body and thickened, cystic iris (*arrow*) and eosinophilic staining in the anterior chamber (**O**) persistent pupillary membrane (PM, *arrow*) and eosinophilic staining in the anterior chamber, (**P**) abnormal and folded retina, (**Q**) lens epithelium is multi-layered (three *arrowheads* on *left*) and there appears to be undifferentiated lens epithelial cells among the lens fibers (*arrowhead* on *right*), (**R**) extensively folded lens capsule (*arrows*; stained with PAS), (**S**) vacuolated lens and abnormal retina with rosettes (RO, *arrow*), (**T**) ectopic ball of retinal cells (RC, *arrow*) between retina and lens. D-ONL, disorganized outer nuclear layer; LC, lens capsule; PM, pupillary membrane; RC, retinal cells; RO, rosette.

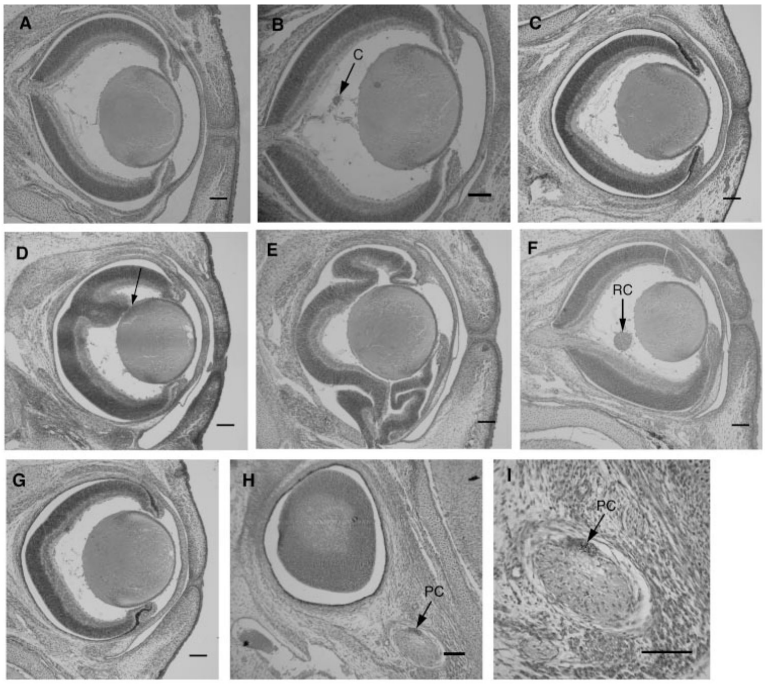


**Figure 3.**

Histologic analysis of E16.5 fetal mouse eyes on two genetic backgrounds. (**A, B**) Wild-type, albino CD1 eyes showing normal histology but with persistent clumps of cells (*arrow*) in the vitreous in (**B**). (**C**) Wild-type pigmented F1 eye showing normal histology. (**D–F**) CD1-*PAX77*$^{+/-}$ eyes with abnormal retinal folding (**D, E**) and ectopic ball (*arrow*) of cells (**F**). (**D**, *arrow*) A retinal fold in contact with the posterior surface of the lens in a region that contains cells with anterior lens epithelial morphology. (**G–I**) F1-*PAX77*$^{+/-}$ eye showing normal morphology (**G**) but ingression of pigmented RPE cells into the optic nerve sheath (*arrow* in **H**; enlarged in **I**, *arrow*). C, clump of cells; PC, pigmented cells; RC, ectopic ball of retinal cells. Scale bar, 100 $\mu$m.

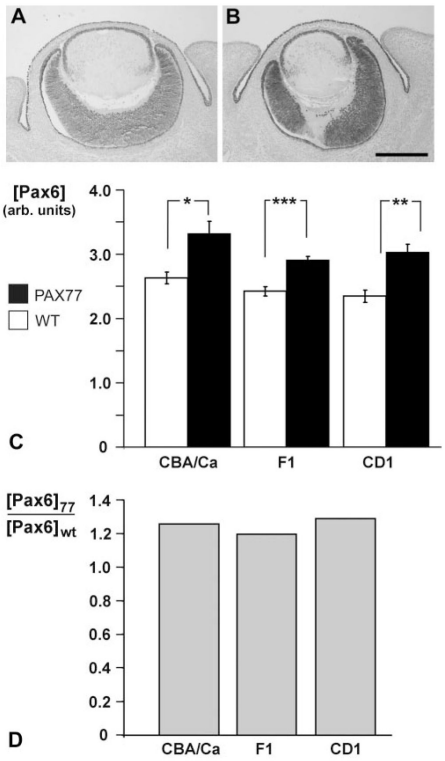


**Figure 4.**

Pax6 expression in *PAX77*$^{+/-}$ eyes. (**A, B**) Pax6 immunohistochemistry of (**A**) an E14.5 wild-type CBA eye and (**B**)an eye of a hemizygous CBA-*PAX77*$^{+/-}$ littermate. (**C, D**) Semiquantitative immunohistochemistry of Pax6 protein levels, normalized using AP2$\alpha$ immunohistochemistry as an internal control. (**C**) Normalized mean Pax6 fluorescence intensity (arbitrary units determined as described in the Methods section) for wild-type lens epithelia and *PAX77*$^{+/-}$ lens epithelia, for different genetic backgrounds. *$P = 0.03$; **$P = 0.001$; ***$P = 0.0002$ ($t$-tests; $n = 4 – 8$ per group). (**D**) The proportionate increase in Pax6 expression in *PAX77*$^{+/-}$ lens epithelia, compared to wild-type, for the different genetic backgrounds. Scale bar, 200 $\mu$m.




Europe PMC Funders Author Manuscripts

Europe PMC Funders Author Manuscripts

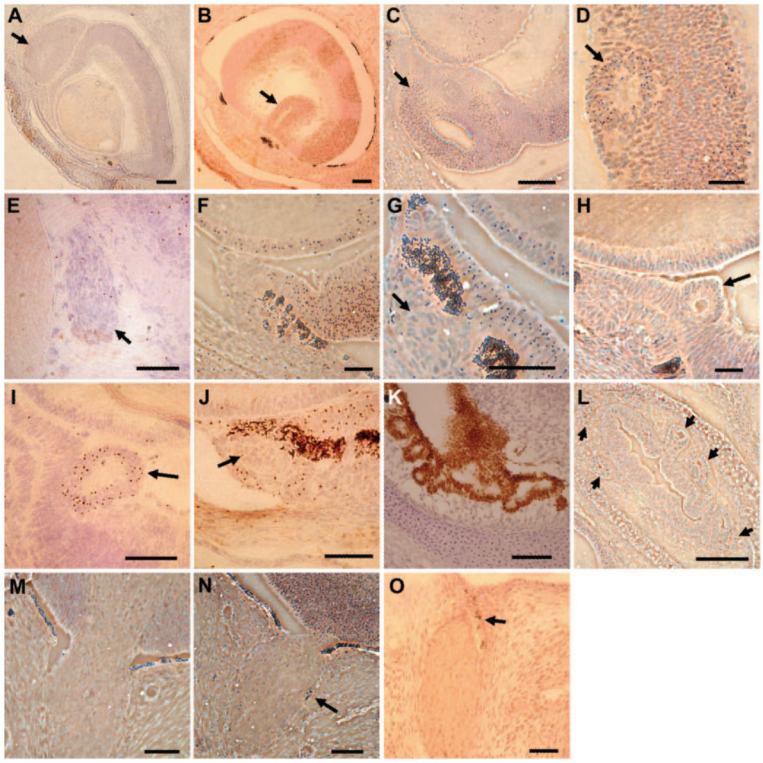


**Figure 5.**

Abnormalities in E16.5 *PAX77*$^{+/-}$↔wild-type chimeras. Retinal abnormalities in E16.5 *PAX77*$^{+/-}$↔wild-type SCA chimeras: Retinal folds (*arrows*) could be composed largely of *PAX77*$^{+/-}$ (*Tg*-negative) cells (**A**) or almost entirely of wild-type (*Tg*$^{+/-}$) cells (**B**), or mixtures of cells of both genotypes (**C**). (**D**) Example of a small vesicle of wild-type (*Tg*$^{+/-}$) cells (*arrow*) within *PAX77*$^{+/-}$ domain of retina. (**E**) Detached group of retinal cells (*arrow*) between the lens and retina of chimera SCA12. Several wild-type (*Tg*-positive) cells were present in the ectopic clump of predominantly *PAX77*$^{+/-}$ (*Tg*-negative) cells. Composition of iris, ciliary body, and lens in E16.5 fetal chimeras: (**F**) SCA control chimera with apparently random distribution of pigmented and *Tg*$^{+}$ cells in different eye tissues. SCA experimental chimeras: (**G**) contribution of *PAX77*$^{+/-}$, *Tg*$^{-/-}$ and *PAX77*$^{-/-}$, *Tg*$^{+/-}$ cells to all tissues (including the lens) and a bud of *PAX77*$^{+/-}$, *Tyr*$^{c/c}$, and *Tg*$^{-/-}$ cells (*arrow*) projecting from the otherwise pigmented iris pigment epithelium. (**H, I**) Buds of *Tg*-positive wild-type (*PAX77*$^{-/-}$, *Tg*$^{+/-}$) cells (*arrows*) in developing ciliary bodies that are otherwise *PAX77*$^{+/-}$, and *Tg*$^{-/-}$. (**J**) Putative segregation of *Tg*-negative, *PAX77*$^{+/-}$ cells (*arrow*) within the trabecular meshwork of an experimental SCA chimera. Serous gland: (**K**) Pax6 immunohistochemical staining of nonchimeric serous gland. (**L**) Partial segregation of *Tg*-negative, *PAX77*$^{+/-}$ cells to larger central serous gland tubules (nasal region) and *Tg*-positive, wild-type cells to smaller tubules (*arrows*). Ingression of RPE cells into the optic nerve heads of experimental chimeras: (**M**) Control SCA chimera showing a sharp boundary between pigmented cells of the RPE and the optic nerve. (**N, O**) Ingression of pigmented cells (*arrow*) into the peripheral sheath of the optic nerve in experimental SCA and SCB chimeras. Because of the composition of the chimeras, the pigmented cells were *PAX77*$^{+/-}$ in the SCB chimera shown in (**N**) but wild-type in the SCA chimera shown in (**O**). Scale bar: (**A, B, C, L**) 100 $\mu$m; (**D, F–K, M–O**) 50 $\mu$m; (**E**) 30 $\mu$m.

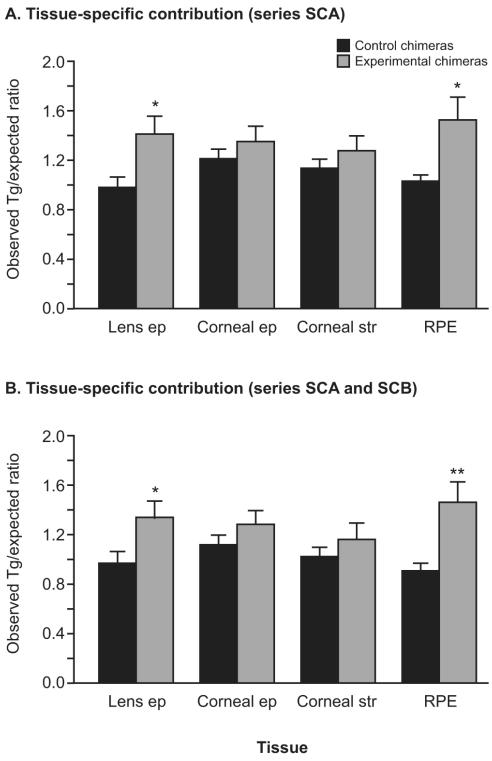


**Figure 6.**

Contribution of *PAX77*$^{+/-}$ cells to four eye tissues in E16.5 fetal chimeras. (**A**) Observed tissue-specific contribution to the lens epithelium, corneal epithelium, corneal stroma (corrected percentage of *Tg*-negative cells) and RPE (percentage of albino cells) in SCA chimeras relative to the expected contribution from the global contribution (percentage of GPI1-A analysis) for each chimera. Comparison of the mean observed/expected ratios in experimental and control chimeras shows a small but significant overrepresentation of *PAX77*$^{+/-}$ cells (high observed/expected ratio) in the lens epithelium and RPE in the 14 experimental chimeric eyes compared with the 10 eyes from control chimeras. (**B**) Histogram showing the overall observed/expected ratios for four eye tissues from 16 experimental chimeric eyes and 12 control chimeric eyes in series SCA and SCB combined. *$P < 0.05$; **$P < 0.01$ by Student's *t*-test. ep, epithelium; str, stroma; RPE, retinal pigment epithelium.

Europe PMC Funders Author Manuscripts





**TABLE 1**

Major Effects of the Genetic Background on *PAX77*$^{+/-}$ Eye Abnormalities

| | Genetic Background | | |
|---|---|---|---|
| **Eye Abnormality** | **CD1** | **CBA** | **F1** |
| Adult | | | |
| Mean percentage of wild-type eye mass | 22% | 60% | 95% |
| Microphthalmia | + | + | − |
| Absent or disorganized ciliary bodies | + | + | + |
| Cystic iris | + | + | + |
| Abnormal retina | + | + | + |
| Small cornea diameter | ± * | + | + |
| Small lens | + | + | ND |
| Cataract | + | + | ND |
| Thickened iris | + | + | − |
| Eosinophilic staining in anterior chamber | + | + | − |
| Ectopic retinal cells posterior to lens | + | ND | ND |
| Persistent pupillary membrane | + | − | − |
| Fetus (E16.5) | | | |
| Ingression of RPE cells into optic nerve sheath | ND † | ND | + |
| Retinal folding | + | ND | − |
| Ectopic retinal cells posterior to lens | + | ND | − |

ND, not done (e.g. because lenses were removed from most F1-*PAX77*$^{+/-}$ and CBA-*PAX77*$^{+/-}$ eyes before embedding for histology).

*Corneal diameter was not obviously disproportionately reduced in the smallest CD1-*PAX77*$^{+/-}$ eyes.

†CD1-*PAX77*$^{+/-}$ mice are albino so any RPE cells in the optic nerve sheath would be less obvious.

Europe PMC Funders Author Manuscripts



*Invest Ophthalmol Vis Sci*. Author manuscript; available in PMC 2010 March 01.



**TABLE 2**

Eye and Nasal Abnormalities and Global Composition of Chimeras (Ranked by Composition)

| Chimera | Abnormality Score | | | Cell Segregation Score* | | | Total Score | % Global Composition | |
|---|---|---|---|---|---|---|---|---|---|
| | Neural Retina Dysgenesis | RPE in Optic Nerve Sheath | Ectopic Group of Retinal Cells | IPE (or Tr Mesh) | Iris or Ciliary Body (NR ep Layer) | Nasal (Serous) Epithelium | | GPI1-A | GPI1-B |
| Experimental *PAX77*$^{+/-}$↔ wild-type chimeras | | | | | | | | | |
| Series SCA | | | | | | | | | |
| SCA13 | 0 | 1 | 0 | 1 | 0 | 0 | 2 | 20.0 | |
| SCA21 | 0 | 2 | 0 | 2 | 0 | 2 | 6 | 40.0 | |
| SCA11 | 1 | 1 | 0 | 1 | 1 | 1 | 5 | 55.1 | |
| SCA17 | 2 | 2 | 0 | 2 | 1 | 2 | 9 | 56.9 | |
| SCA18 | 2 | 2 | 0 | 0 | 1 | 1 | 6 | 68.9 | |
| SCA15 | 2 | 2 | 0 | 0 | 2 | 1 | 7 | 76.9 | |
| SCA12 | 2 | 2 | 1 | 0 | 1 | 2 | 8 | 87.2 | |
| Series SCB | | | | | | | | | |
| SCB9 | 0 | 2 | 0 | 0 | 0 | 2 | 4 | | 50.1 |
| Frequency | 9/16 | 14/16 | 1/16 | 6/16 | 6/16 | 11/16 | | | |
| Percentage | 56 | 88 | 6 | 38 | 38 | 69 | | | |
| Control *PAX77*$^{+/-}$↔ wild-type chimeras | | | | | | | | | |
| Series SCA | | | | | | | | | |
| SCA19 | 0 | (2)† | 0 | 0 | 0 | 0 | (2) | 28.6 | |
| SCA20 | 0 | 0 | 0 | 0 | 0 | 0 | 0 | 62.1 | |
| SCA16 | 0 | 0 | 0 | 0 | 0 | 0 | 0 | 62.2 | |
| SCA14 | 0 | 0 | 0 | 0 | 0 | 0 | 0 | 71.1 | |
| SCA23 | 0 | 0 | 0 | 0 | 0 | 0 | 0 | 84.7 | |
| Series SCB | | | | | | | | | |
| SCB11 | 0 | 0 | 0 | 0 | 0 | 1 | 1 | | 12.7 |
| SCB17 | 0 | (1)† | 0 | 0 | 0 | 0 | (1) | | 52.0 |
| Frequency | 0/14 | (3)/14 | 0/14 | 0/14 | 0/14 | 1/14 | | | |
| Percentage | 0 | (21) | 0 | 0 | 0 | 7 | | | |

Europe PMC Funders Author Manuscripts

The total abnormality/segregation score in *PAX77*$^{+/-}$↔wild-type chimeras showed a significant correlation (Kendall $\tau = 0.618$; $P = 0.032$) with the global composition (% GPI1-A or %GPI1-B depending which is produced by the *PAX77*$^{+/-}$ cells). IPE, iris pigment epithelium; RGCs, retinal ganglion cells RPE, retinal pigment epithelium; Tr mesh, trabecular meshwork; NR ep layer, epithelial layer of iris and ciliary body that extends from the neural retina.

*Abnormality or cell segregation score: 0, absent; 1, present unilaterally; 2, present bilaterally.

†Only individual RPE cells were present in the optic nerve sheath of control chimeras.

Europe PMC Funders Author Manuscripts





**TABLE 3**

Comparison of Eye Abnormalities Reported for *Pax6*$^{+/-}$ (e.g. *Pax6*$^{Sey/+}$ or *Pax6*$^{Sey\text{-}New/+}$) and *PAX77*$^{+/-}$ Genotypes

| **Eye Abnormality**[*] | ***Pax6*** $^{+/-}$ | ***PAX77*** $^{+/-}$ |
|---|---|---|
| Similarities between *Pax6*$^{+/-}$ and *PAX77*$^{+/-}$ | | |
| Microphthalmia | Yes[†] | Yes24,42[‡] |
| Small abnormal lens with cataracts | Yes10,43 | Yes24[‡] |
| Folded lens capsule | Yes43 | Yes[‡] |
| Multilayered lens epithelium | Yes43 | Yes24[‡] |
| Retinal dysplasia | Yes18 | Yes24[‡] |
| Adhesions in the anterior chamber (±obstruction of the angle) | Yes16,18 | Yes[‡] |
| Abnormal cell accumulation in the vitreous | Yes18 | Yes[‡] |
| Differences between *Pax6*$^{+/-}$ and *PAX77*$^{+/-}$ | | |
| Absent or reduced irides (±coloboma) | Yes2 | No24,42[‡] |
| Persistent bridge of cells between cornea epithelium and lens | Yes10,14,15,43 | No[‡] |
| Fusion of lens and corneal stroma (central corneal endothelium lost) | Yes18 | No[‡] |
| Thin corneal epithelium[§] | Yes16,19 | No42[‡] |
| Corneal opacity with stromal vascularisation and cellular infiltrates | Yes16,18 | No42[‡] |
| Presence of goblet cells in the corneal epithelium | Yes16 | No42[‡] |
| Cystic and thickened irides | No | Yes24,42[‡] |
| Persistent pupillary membrane | No | Yes[§] |
| Small, abnormal or absent ciliary bodies | No | Yes24,42[‡] |
| Disproportionately reduced corneal diameter | No | Yes24,42[‡] |
| Ingression of RPE cells into optic nerve sheath | No/ND | Yes[‡] |

[*] Penetrance of some abnormal eye phenotypes depends on genetic background (see text). Yes = feature reported for at least one genetic background; No = feature not reported; No/ND = feature not reported (but probably not done).

[†] References 2, 10, 14-16, 18, 19, 43, 44.

[‡] Present study.

[§] See Dorà et al.42 for more detailed comparison of *Pax6*$^{+/-}$ and *PAX77*$^{+/-}$ corneas.

Europe PMC Funders Author Manuscripts





*Invest Ophthalmol Vis Sci*. Author manuscript; available in PMC 2010 March 01.

**TABLE 4**

Comparison of Effects on E16.5 Fetal Eyes in *Pax6*$^{+/-}$↔Wild-Type and *PAX77*$^{+/-}$↔Wild-Type Chimeras

| Tissue | *Pax6*$^{+/-}$↔Wild-Type Chimeras (Collinson et al.14) | *PAX77*$^{+/-}$↔Wild-Type Fetal Chimeras (Present Study) |
|---|---|---|
| Morphological abnormalities | | |
| Optic nerve/retina boundary | None | RPE cells in optic nerve sheath |
| Neural retina | None | Retinal dysgenesis and ectopic balls of RGCs |
| Probably nonautonomous effects | | |
| Optic nerve/retina boundary | None | *PAX77*$^{+/-}$ and wild-type RPE cells in ONS |
| Neural retina | None | *PAX77*$^{+/-}$ and wild-type cells in retinal folds (also wild-type cells among ectopic balls of *PAX77*$^{+/-}$ RGCs [*]) |
| Cell-autonomous effects | | |
| Lens epithelium | *Pax6*$^{+/-}$ cells excluded [†] | *PAX77*$^{+/-}$ cells overrepresented |
| RPE | None | *PAX77*$^{+/-}$ cells overrepresented |
| Neural retina, iris pigment epithelium, ciliary body and iris NR ep layer | None | Some segregation of *PAX77*$^{+/-}$ and wild-type cells |

NR ep layer, epithelial layer of iris and ciliary body that extends from the neural retina; ONS, optic nerve sheath; RGCs, retinal ganglion cells; RPE, retinal pigment epithelium.

[*] Further work is needed to determine whether the effect is cell-autonomous or nonautonomous.

[†] *Pax6*$^{+/-}$ cells were excluded from the lens epithelium in the first study of *Pax6*$^{+/-}$↔wild-type chimeras.14 A more recent study showed that *Pax6*$^{+/-}$ cells could contribute to the lens epithelium of *Pax6*$^{+/-}$↔wild-type chimeras,30 but it was unclear whether they were depleted because the contribution of *Pax6*$^{+/-}$ cells was not quantified.